

STRAND: Sequence-Conditioned Transport for Single-Cell Perturbations

Boyang Fu¹ George Dasoulas² Sameer Gabbita³ Xiang Lin¹ Shanghua Gao¹ Xiaorui Su¹ Soumya Ghosh²
Marinka Zitnik^{1,4,5,6}

Abstract

Predicting how genetic perturbations change cellular state is a core problem for building controllable models of gene regulation. Perturbations targeting the same gene can produce different transcriptional responses depending on their genomic locus, including different transcription start sites and regulatory elements. Gene-level perturbation models collapse these distinct interventions into the same representation. We introduce STRAND, a generative model that predicts single-cell transcriptional responses by conditioning on regulatory DNA sequence. STRAND represents a perturbation by encoding the sequence at its genomic locus and uses this representation to parameterize a conditional transport process from control to perturbed cell states. Representing perturbations by sequence, rather than by a fixed set of gene identifiers, supports zero-shot inference at loci not seen during training and expands inference-time genomic coverage from $\sim 1.5\%$ for gene-level single-cell foundation models to $\sim 95\%$ of the genome. We evaluate STRAND on CRISPR perturbation datasets in K562, Jurkat, and RPE1 cells. STRAND improves discrimination scores by up to 33% in low-sample regimes, achieves the best average rank on unseen gene perturbation benchmarks, and improves transfer to novel cell lines by up to 0.14 in Pearson correlation. Ablations isolate the gains to sequence conditioning and transport, and case studies show that STRAND resolves functionally alternative transcription start sites missed by gene-level models.

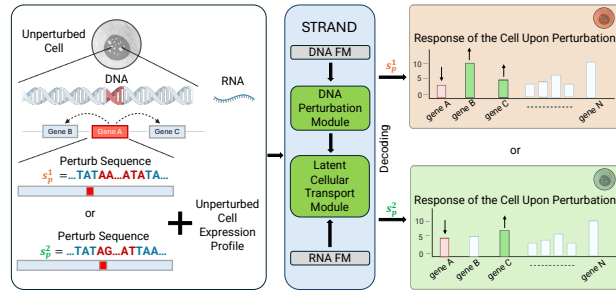


Figure 1. Overview of STRAND. STRAND conditions perturbation effects on regulatory DNA sequence, to perform in-silico profiling of locus-specific perturbations at nucleotide resolution. Perturbations targeting the same gene at different genomic locations (s_p^1, s_p^2) can induce distinct transcriptional responses.

1. Introduction

Predicting how genetic perturbations change cellular state is a core problem for building controllable models of gene regulation (Roohani et al., 2023; Lotfollahi et al., 2023b; Ahlmann-Eltze et al., 2025; Adduri et al., 2025b; Park & Li, 2026; Lorch et al., 2026; Dong et al., 2026). In practice, regulatory effects are mediated by specific DNA sequences, such as promoters, enhancers, and alternative transcription start sites (TSS), rather than by genes as indivisible units (Nasser et al., 2021; Avsec et al., 2021; Linder et al., 2025; Pampari et al., 2025; Avsec et al., 2026). However, most existing single-cell perturbation models, including recent single-cell foundation models, represent perturbations at the gene level (Cui et al., 2024; Wenkel et al., 2025; Pasigan et al., 2025; Zhu & Li, 2025; Dong et al., 2026), either as discrete identifiers or as static nodes in a graph. As a result, perturbations that target different genomic loci within the same gene are mapped to the same representation. This creates a resolution gap: experimental technologies such as CRISPR-i/a and base editing can intervene at precise genomic locations, while predictive models treat all interventions within a gene body as equivalent.

This resolution gap matters because perturbations sharing the same gene label can produce vastly different cellular outcomes depending on which regulatory sequence is targeted. For example, disrupting the coding region of gene *BCL11A* is lethal to cells, whereas targeting a specific enhancer sequence induces therapeutic effects without harming the

¹Department of Biomedical Informatics, Harvard Medical School, Boston, MA, USA ²Merck & Co., Inc., Cambridge, MA, USA ³Department of Biomedical Engineering, Johns Hopkins University, Baltimore, MD, USA ⁴Kempner Institute for the Study of Natural and Artificial Intelligence, Harvard University, Allston, MA, USA ⁵Broad Institute of MIT and Harvard, Cambridge, MA, USA ⁶Harvard Data Science Initiative, Cambridge, MA, USA. Correspondence to: Marinka Zitnik <marinka@hms.harvard.edu>.

cell (Smith et al., 2017; Frangoul et al., 2021). Even within a single enhancer, only a small subset of nucleotides actually controls gene regulation; perturbing nearby positions often has no measurable effect (Canver et al., 2015). These observations motivate modeling perturbations at sequence-level resolution. Such resolution is also essential for modeling the 98% of the genome that lies outside protein-coding regions, where most disease-associated genetic variants reside but remain inaccessible to gene-level perturbation models (Maurano et al., 2012; Nasser et al., 2021).

Modeling perturbation responses at nucleotide resolution is difficult for several reasons. (1) First, *the input space is large*: regulatory effects can depend on hundreds of thousands of nucleotides, and the mapping from raw DNA sequence to transcriptomic change is highly non-linear (Cheng et al., 2025; Fu et al., 2023). Recent DNA foundation models learn general regulatory grammar from sequence (Linder et al., 2025; Avsec et al., 2026; Patel et al., 2024), but they are trained to predict regulatory signals, not perturbation-induced state changes. As a result, perturbation effects must be inferred indirectly through post-hoc analyses and remain limited to local sequence windows, without modeling how perturbations propagate through cell-type-specific regulatory programs (Wei et al., 2025). (2) Second, *regulatory effects are context-dependent*. The impact of a sequence motif depends on chromatin state, long-range interactions, and cellular context, all of which vary across cell types (Song et al., 2025). Capturing this dependence requires linking sequence-level changes to transcriptional (RNA) responses conditioned on cellular state. (3) Third, *the space of possible sequence perturbations is combinatorial*, while available single-cell perturbation data is sparse across perturbations, samples, and contexts (Peidli et al., 2024; Huang et al., 2025), which makes direct supervision from DNA sequence to perturbation response infeasible.

Most existing perturbation predictors avoid modeling upstream regulatory mechanisms and instead condition on proxy descriptors of the perturbed gene, including discrete covariates (Bereket & Karaletsos, 2023; Tu et al., 2024; Gaudelet et al., 2024), protein function (Adduri et al., 2025b; Dong et al., 2026), gene regulatory structure (Wu et al., 2022; Roohani et al., 2023; Wenkel et al., 2025), or text-derived embeddings (Wu et al., 2025; Zhu & Li, 2025). DNA and genome language models learn general sequence representations, but they are not trained to predict perturbation-induced transcriptomic state changes, so they do not provide a direct perturbation predictor. These designs can interpolate within a fixed set of genes, but they impose a closed perturbation vocabulary defined by gene identifiers. Generalization to unseen perturbations then relies on transferring gene-level correlations, which often yields limited gains over simple baselines (Wu et al., 2024). More importantly, gene-identifier conditioning cannot represent

locus-defined perturbations (Table 1).

Present Work. We introduce STRAND, a generative model that formulates perturbation prediction as a sequence-conditioned transport problem (Figure 1). The model takes as input an unperturbed (control) cell state and the DNA sequence at a target genomic locus, and predicts the distribution of cellular states after perturbation at that locus. Unlike sequence-to-expression models that predict predefined regulatory tracks over local sequence windows, STRAND connects genomic sequence to global transcriptomic state changes. By representing perturbations as continuous functions of nucleotide sequence rather than as gene identifiers, the model supports zero-shot prediction at arbitrary genomic coordinates and can distinguish perturbations targeting different regulatory elements within the same gene. To address the scarcity of labeled perturbation responses, STRAND integrates sequence and expression representations through a sequence-conditioned perturbation module and a transport-based generative model. The perturbation module maps DNA sequence representations to the latent space of an RNA encoder, producing a perturbation embedding that conditions a latent diffusion process transporting control cell distributions to perturbed distributions.

Our contributions:

- STRAND maps DNA embeddings at the target locus into the RNA latent space to form regulatory-context-aware perturbation representations, improving Pearson correlation on top differentially expressed genes by 0.08-0.12 over baselines without sequence conditioning.
- We formulate perturbation prediction as sequence-conditioned generative transport from unperturbed to perturbed cell-state distributions using latent diffusion, rather than deterministic regression. Relative to a predictor without transport, this reduces Energy Distance by 38.9% and increases mean R^2 by 27.6% on the multi-cell-line setting.
- We model perturbations as functions of genomic sequence instead of gene identifiers, enabling zero-shot inference at unseen loci and locus-resolved in-silico profiling. This expands inference-time genomic coverage from $\sim 1.5\%$ for gene-level models to $\sim 95\%$ of the genome, improves discrimination scores by up to 33%, achieves best average rank on unseen-gene benchmarks, and improves transfer to unseen cell lines by up to 0.14 in Δ Pearson.

2. Related Work

Single-Cell Perturbation Prediction. Early single-cell perturbation predictors model intervention effects by conditioning a function approximator on a perturbation identifier or learned embedding and regressing perturbed expression from control states. Counterfactual methods such as scGen, CPA, and SAMS-VAE learn latent spaces in

Table 1. Perturbation modeling comparison. Gene-level methods operate at ~ 27 kb resolution and are restricted to protein-coding regions ($\sim 1.5\%$ of the genome); DNA foundation models do not predict perturbation responses. STRAND supports genome-wide perturbation prediction at 0.1 kb resolution

Method	Unit	Res.	Coverage
GEARS	Gene	~ 27 kb	$\sim 1.5\%$ genome
BioLord	Gene	~ 27 kb	$\sim 1.5\%$ genome
STATE	Gene	~ 27 kb	$\sim 1.5\%$ genome
RNA FMs	Gene	~ 27 kb	$\sim 1.5\%$ genome
DNA FMs	Sequence	N/A	N/A
STRAND	Sequence	0.1 kb	Whole genome

which perturbations correspond to approximately additive shifts (Lotfollahi et al., 2019; 2023a; Bereket & Karaletsos, 2023). Graph- and relation-aware models, including graphVCI, GEARS, CellOracle, BioLord, and PertAdapt impose structure on the perturbation space using gene-gene or regulatory networks (Wu et al., 2022; Roohani et al., 2023; Kamimoto et al., 2023; Piran et al., 2024; Bai et al., 2025). Recent “virtual cell” models, such as TxPert, STATE, and STACK, improve prediction accuracy and outperform earlier approaches like CPA across several gene perturbation benchmarks (Adduri et al., 2025a; Wenkel et al., 2025; Dong et al., 2026). However, benchmarks show that increased model complexity does not improve perturbation signal recovery: many methods struggle to learn meaningful effects, exhibit mode collapse, or fail to disentangle batch effects (Wu et al., 2024; Viñas Torné et al., 2025; Ahlmann-Eltze et al., 2025; Luecken et al., 2021). Perturbation modeling remains an open problem, with ongoing work focused on generalization (Wang et al., 2023; Tu et al., 2024). In contrast, STRAND conditions perturbation prediction on regulatory DNA context, treating a perturbation as a structured transformation of a cell population rather than as a static identifier or relational proxy.

DNA Sequence Models. DNA foundation models trained on regulatory tracks learn sequence features that predict chromatin accessibility, transcription factor binding, and gene expression and isoforms (Avsec et al., 2021; Lal et al., 2024; Garau-Luis et al., 2024; Linder et al., 2025; Avsec et al., 2026). They provide strong sequence representations, but using them for perturbation-response prediction is not straightforward. First, these models are sequence-to-function predictors: given a DNA sequence (optionally with a cellular context), they output regulatory readouts at predefined loci. Simulating a perturbation therefore requires comparing predictions on reference versus edited sequences, a post-hoc differencing procedure that treats perturbations implicitly rather than as explicit interventional variables (Wei et al., 2025). Second, their prediction heads operate over fixed genomic windows (typically tens to hundreds of kilobases), which limits inference to local effects and does not

model genome-wide transcriptomic shifts. Third, cell-type conditioning is limited to contexts observed during training, restricting generalization to unseen cellular states. Conversely, most single-cell perturbation models operate in expression space and do not use DNA sequence information to define perturbation semantics.

Generative Distribution Modeling. Recent methods model heterogeneous perturbed cell distributions through conditional diffusion (SquiDiff (He et al., 2025a), scDiffusion (Luo et al., 2024; Guo et al., 2023)) or optimal transport formulations (CellOT (Bunne et al., 2023), CellFlow (Klein et al., 2025), Schrödinger bridges (Liu et al., 2023a), TrajectoryNet (Tong et al., 2020), cMonge (Driessen et al., 2025)). However, these approaches either condition on cell-state metadata or drug/treatment information, requiring separate training transport functions for each perturbation or dataset, preventing unified generalization. STRAND addresses this limitation by learning a single transport function in a cellular latent space that conditions on DNA embeddings, enabling generalization across both perturbation sites and cell types.

Causal and Disentanglement Methods. Methods, such as LCD (Lorch et al., 2026), CINEMA-OT (Dong et al., 2023), and XTransferCDR (Liu & Jin, 2025), provide frameworks for perturbation modeling, including causal structure recovery and confounder-aware transport. However, they operate at the gene level and represent perturbations as abstract identifiers, so they cannot distinguish regulatory contexts within the same gene. STRAND instead conditions transport on regulatory DNA embeddings, allowing the model to represent where a perturbation acts within a gene.

Single-Cell Foundation Models for Genetic Perturbations. Single-cell foundation models such as Geneformer, scGPT, and scFoundation (Theodoris et al., 2023; Cui et al., 2024; Hao et al., 2024), as well as text-based models such as PerturbQA and rbio1 (Wu et al., 2025; Zhu & Li, 2025; Istrate et al., 2025), learn cell representations but typically condition on perturbation names or identifiers and operate only on single-cell measurements. Reliance on coarse identifiers may also explain why such architectures have not consistently outperformed linear baselines (Ahlmann-Eltze et al., 2025). STRAND combines single-cell modeling via an RNA foundation model (Heimberg et al., 2025) with perturbation semantics grounded in sequence representations from DNA foundation models.

Chemical vs. Genetic Perturbations. Drug-response modeling has advanced through benchmarks such as OP3 (Szałata et al., 2024) and generative approaches including scPPDM and SquiDiff (Liang et al., 2025; He et al., 2025b) that condition on molecular graphs. While some methods model chemical and genetic perturbations (Hetzell et al., 2022; Yu et al., 2025; Gonzalez et al., 2025), models

rely on dose-response assumptions and molecular similarity rather than DNA context. We therefore focus comparisons on genetic perturbation methods, treating chemical models as complementary evidence for distributional modeling.

3. Methods

3.1. Problem Setup

Let $\mathbf{x} \in \mathbb{R}^G$ denote the log-normalized gene expression profile of a single cell. We consider two empirical distributions over cell states: a control cell distribution $\mathbf{x}_c \sim p_0(\mathbf{x})$ and a perturbed cell distribution $\mathbf{x}_p \sim p_1(\mathbf{x} \mid s, \mathbf{m})$, where $s \in \mathcal{A}^w$ denotes the local genomic sequence ($\mathcal{A} = \{A, C, G, T\}$) and \mathbf{m} is a binary vector that specifies the perturbed nucleotide positions (e.g., a CRISPR target loci) within that sequence, with 1 indicating perturbation region. More explanation on this design choice can be seen at App. B.4.

We utilize a pretrained RNA foundation model, denoted as encoder e_ψ , to map cells into a shared latent space $\mathbf{z} = e_\psi(\mathbf{x}) \in \mathbb{R}^d$. Accordingly, we denote $\mathbf{z}_c = e_\psi(\mathbf{x}_c)$ and $\mathbf{z}_p = e_\psi(\mathbf{x}_p)$. Similarly, a pretrained DNA foundation model maps the raw sequence s to token embeddings $\mathbf{E}_s \in \mathbb{R}^{L \times d_0}$ using the backbone layer of the U-net in Flashzoi. Where $L = \frac{w}{B}$, where the raw sequence has fixed length $w = 524, 288$, and $B = 128$.

Our goal is to learn a conditional transport model $\mathbf{z}_p \sim \mathcal{G}_\theta(\mathbf{z}_c, s, \mathbf{m})$ which transports a control latent \mathbf{z}_c to a perturbed latent \mathbf{z}_p conditioned on the specific perturbation parameters. Since the control-perturbation cells are unpaired, we use a scalable Optimal Transport (OT) (Halmos et al., 2025) to pair the data. Details are discussed in App. A.

3.2. Sequence-Conditioned Perturbation Module

We model perturbations as interventions localized at specific genomic coordinates, leveraging pre-trained DNA embeddings as a knowledge base of regulatory activity. A perturbation is defined by a binary mask $\mathbf{m} \in \{0, 1\}^L$ over sequence positions. Given sequence embeddings $\mathbf{E}_s \in \mathbb{R}^{L \times d}$ and perturbation mask \mathbf{m} , the DNA Perturbation Module produces a perturbation embedding $\mathbf{u}_p = g_\phi(\mathbf{E}_s, \mathbf{m})$ that encodes both the local regulatory context at the perturbation site and its interaction with the broader genomic landscape.

Perturbation-Anchored Query Construction: We first extract a query vector representing the perturbed region. Let $\mathcal{P} = \{i \mid m_i = 1\}$ denote the set of perturbed positions. The query is constructed by mean-pooling embeddings within this region and projecting to a learned representation: $\mathbf{q}_p = \text{MLP}\left(\frac{1}{|\mathcal{P}|} \sum_{i \in \mathcal{P}} \mathbf{E}_{s,i}\right)$. This transformation compresses the regulatory features of the targeted region into a compact representation suitable for querying contextual information.

Cross-Attention over Sequence Context: Perturbation effects depend not only on the targeted region but also on the surrounding regulatory landscape. To capture this dependency, we employ single-query multi-head cross-attention from the perturbation query \mathbf{q}_p to the full sequence embedding \mathbf{E}_s :

$$\alpha_j = \text{softmax}_j \left(\frac{(\mathbf{q}_p W_Q)(\mathbf{E}_{s,j} W_K)^\top}{\sqrt{d_k}} + b_j \right),$$

$$\mathbf{h}_p = \sum_{j=1}^L \alpha_j (\mathbf{E}_{s,j} W_V),$$

where W_Q, W_K, W_V are learned projection matrices and b_j is a learned positional bias that encodes structural priors (e.g., distance from the perturbation site).

Perturbation Embedding Construction: The final perturbation embedding combines the local regulatory features of the perturbed region with its broader genomic context: $\mathbf{u}_p = \text{Proj}([\mathbf{q}_p \parallel \mathbf{h}_p])$, where $\text{Proj}(\cdot)$ is a two-layer MLP with layer normalization and GELU activation.

3.3. Latent Generative Module

Generative transport from control to perturbation: We model perturbation response as a distributional transport problem rather than a regression task to improve the generation heterogeneity and preserve biological patterns. Concretely, we learn a stochastic transition that maps each control latent \mathbf{z}_c into an OT paired perturbed latent \mathbf{z}_p . A key design choice is to anchor generation on observed control cells so the model learns how a perturbation changes a cell state instead of generating from an unconditional noise prior. This “control-anchored” generative design is especially important in multi-cell-line settings, where perturbation effects are defined relative to different basal states. We implement this idea using an interpolation-based conditional diffusion objective (I2SB) (Liu et al., 2023b), constructing a stochastic interpolant between the paired latents:

$$\mathbf{z}_t = w_0(t)\mathbf{z}_p + w_1(t)\mathbf{z}_c + \sigma(t)\boldsymbol{\epsilon}, \quad (1)$$

$$\boldsymbol{\epsilon} \sim \mathcal{N}(0, \mathbf{I}), \quad t \in \{0, \dots, T\},$$

where $w_0(t), w_1(t)$ and $\sigma(t)$ are determined by the I2SB noise schedule via σ_t^2 and $\bar{\sigma}_t^2$ (see App. B). We learn a conditional noise prediction network $\boldsymbol{\epsilon}_\theta(\mathbf{z}_t, t, \mathbf{u}_p, \mathbf{z}_c)$ to approximate the vector field driving this transport. The prediction network is trained via Bridge Matching:

$$\mathcal{L}_{\text{bridge}} = \mathbb{E}_{\mathbf{z}_p, \mathbf{z}_c, t} \left[\left\| \boldsymbol{\epsilon}_\theta(\mathbf{z}_t, t, \mathbf{u}_p, \mathbf{z}_c) - \boldsymbol{\epsilon}^{\text{I2SB}} \right\|_2^2 \right],$$

with $\boldsymbol{\epsilon}^{\text{I2SB}} \doteq \frac{\mathbf{z}_t - \mathbf{z}_p}{\sigma_t}$. This training objective follows I2SB (Liu et al., 2023b), with full derivations in App. B. This formulation enables STRAND to generate perturbed states by transporting control states under sequence-conditioned perturbation semantics. $\boldsymbol{\epsilon}_\theta$ learns a guided diffusion process

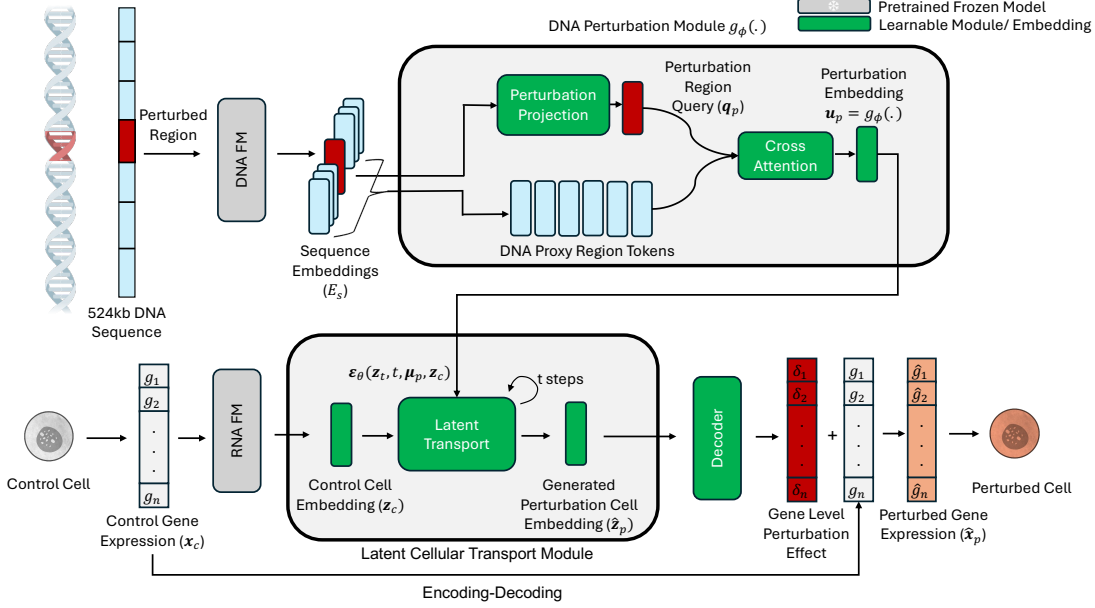


Figure 2. STRAND architecture design. The framework integrates genomic and transcriptomic modalities to predict perturbed cell expression. The pipeline consists of three main learnable components: (1) A **DNA Perturbation Module** $g_\phi(\cdot)$ that processes representations from a frozen Borzoi model and perturbation masks to produce the perturbation embedding μ_p ; (2) A **Latent Cellular Transport Module** utilizing latent diffusion, $\epsilon_\theta(z_t, t, \mu_p, z_c)$, to synthesize the perturbation cell embedding \hat{z}_p conditioned on the control cell embedding; and (3) A **Gene Level Decoding Module** that projects the synthesized latent features to the final predicted perturbed expression.

conditioned jointly on the control state z_c and the sequence embedding u_p , such that the influence of a given DNA perturbation is modulated by the baseline cellular state, yielding cell-type-specific transition dynamics.

RNA Expression Decoding. We decode via a residual decoder D_ξ : first forms a smooth baseline $\hat{x}_c := d_\eta(e_\eta(x_c))$ using a lightweight MLP autoencoder, then predict $\hat{x}_p = \hat{x}_c + D_\xi(\hat{z}_p)$, where \hat{z}_p is denoised (single-step denoising during training; multi-step at inference). The reconstruction loss \mathcal{L}_{rec} uses a hurdle log-normal likelihood to model zero inflation (App. D).

Alignment of DNA Sequence to RNA Expression. We align the sequence-derived perturbation embedding \bar{u}_k with the mean RNA latent displacement $\Delta \bar{z}_k$ using a CLIP-style contrastive loss (Radford et al., 2021):

$$\mathcal{L}_{\text{align}} = \text{CLIP}(\text{Proj}_{\text{DNA}}(\bar{u}_k), \Delta \bar{z}_k), \quad (2)$$

where Proj_{DNA} maps sequence features to the RNA latent space. We estimate $\Delta \bar{z}_k$ with EMA and use RNA-similarity soft targets (App. C).

3.4. Overall STRAND Objective

The model is trained end-to-end by minimizing a weighted sum of the bridge matching, reconstruction, and alignment losses as: $\mathcal{L} = \lambda_1 \mathcal{L}_{\text{bridge}} + \lambda_2 \mathcal{L}_{\text{CLIP}} + \lambda_3 \mathcal{L}_{\text{rec}}$. We employ uncertainty weighting (Kendall et al., 2018) to dynamically

adjust λ_i during training.

3.5. Modular Design of STRAND

Our architecture treats the pretrained DNA and RNA foundation models as modular components that can be substituted with alternative encoders. In this work, we use Flashzoi/Borzoi (Linder et al., 2025; Hingerl et al., 2025) for DNA embeddings and SCimilarity (Heimberg et al., 2025) for RNA representations, chosen for their demonstrated performance on regulatory prediction and cell-type annotation tasks, respectively. STRAND can easily adapt alternative DNA encoders (Avsec et al., 2026; 2021), and RNA encoders (Cui et al., 2024; Hao et al., 2024).

4. Experimental Setup

Data Source and Preprocessing. We utilize single-cell perturbation datasets from PerturbQA (Wu et al., 2025), spanning four cell lines. We restrict our analysis to K562, Jurkat, and RPE1, excluding HepG2 due to low statistical power for differential expression evaluation arising from reduced cell counts per perturbation (median 45 cells in HepG2 versus 72 in RPE1, 83 in Jurkat, and 121 in K562 (Nadig et al., 2025)). We further constructed a cross-cell-line dataset (termed *Combined*) using the three cell lines, with details at App. H.1. For STRAND, we couple control and perturbed cells using Optimal Transport (OT), with details at App. A.

State-of-the-Art Methods. Perturbation prediction remains a challenging problem where no method consistently dominates across evaluation settings (Viñas Torné et al., 2025; Ahlmann-Eltze et al., 2025; Wu et al., 2024). We therefore structure our evaluation around five complementary baselines: *GEARS* (Roohani et al., 2023), *BioLord* (Piran et al., 2024), *STATE* (Adduri et al., 2025b), *Linear* (Linder et al., 2025), and *PerturbMean* (Viñas Torné et al., 2025). Implementation details for all baselines are provided in App H.

Evaluation Metrics. We adopt evaluation protocols tailored to each experimental setting.

For models trained and evaluated on individual cell lines, we adhere to the benchmarking standards established by the Virtual Cell Challenge and the STATE framework (Adduri et al., 2025b). For each test perturbation, we sample $N = 256$ random control cells from the corresponding cell line. Each model will generate the predicted perturbed population \hat{p}_1 , with the same sample size, which is compared against the ground-truth distribution. Following the CellEval framework (Adduri et al., 2025b), we evaluate performance along three complementary axes: (i) **Global Fit** (MSE, Δ Pearson), (ii) **DE Signal** (Dir. Match, Prec. @ N, Ov. @ N), and (iii) **Distributional Fidelity** (Discr. Cos (Wu et al., 2024)). We exclude metrics that treat Wilcoxon-based DE calls as hard ground-truth labels (e.g., DE classification or recall-based metrics), which have been shown to produce severely inflated false discoveries (Squair et al., 2021; Murphy et al., 2023).

For joint-cell-line (*Combined*), we additionally reported metrics assessing the distributional fidelity and population-level accuracy following (Klein et al., 2025) on settings not natively supported by CellEval. We evaluate **Energy Distance** and **pseudo-bulk R^2** following a similar protocol as in (Klein et al., 2025). Detailed metric definitions are provided in App. F.2.

5. Results

5.1. Gene-Level Perturbation Prediction

Low-Sample Gene Perturbation. To model realistic data scarcity, we allow a small amount of supervision for each gene perturbation to be tested by moving $k = 5$ cells per test gene from the original test set into the training set. Models are trained independently on each cell line and evaluated on the corresponding held-out test cells. More details on the train/ test data are at App. F.1.

As shown in Table 2, S5, STRAND achieves the best **average rank** (1.57-1.71) across all metrics and cell lines. GEARS achieves competitive E-Distance by leveraging gene-gene interaction graphs, but cannot support joint multi-cell-line training or transfer to unseen cell lines. On the *Com-*

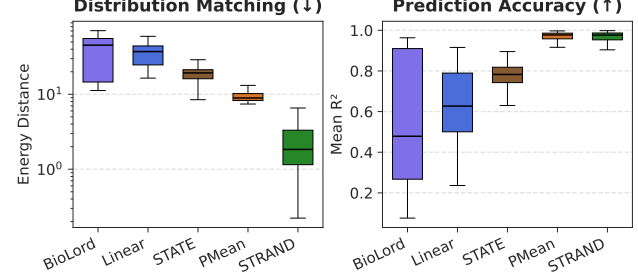


Figure 3. SOTA methods Benchmark on Low-Sample Gene Perturbation. STRAND is compared against PMean (PerturbMean), STATE, Linear, and Biolord on the *Combined* data. GEARS is excluded as it doesn't support cross-cell-line joint training.

bined dataset with joint training (Figure 3), STRAND reduces E-distance by $4 \times$ compared to the next-best method.

Baseline methods exhibit a performance trade-off: simple methods (Linear, PerturbMean) achieve low MSE but poor discrimination (score ≈ 0.5), while deep learning methods (STATE) capture heterogeneity but suffer in capturing global pattern (highest MSE and E-Distance). STRAND unifies both strengths, matching simple baselines' global accuracy (MSE ≈ 0.78 in K562) while improving discrimination by 33% over STATE (0.72 vs 0.54). On combined data (Figure 3), STRAND maintains comparable MSE to PerturbMean while reducing E-Distance > 4 -fold.

Zero-shot Unseen Perturbation. We next investigate STRAND's generalizability to unseen contexts.

Unseen Gene Perturbation. Similarly to before, we adopt the train-test splits provided by PerturbQA (Wu et al., 2025). In this setting, methods are trained exclusively on a designated set of perturbations without access to test labels or test expression profiles (see App. F.1 for data details).

We compare STRAND with all SOTA algorithms except STATE, which requires the perturbation to be seen for at least one cellular context to make a prediction, and does not support zero-shot generalization to unseen perturbations (Adduri et al., 2025b). As shown in Table 2, S6, STRAND achieves the state-of-the-art performance with overall best rank. Notably, across all settings, STRAND achieves the highest Discrimination Scores. This metric highlights the model's ability to capture nuanced biological heterogeneity and its robustness against mode collapse (Wu et al., 2024), abilities we attribute to our specialized DNA perturbation module and generative process.

Unseen Cell-Line Perturbation. Next, we evaluate STRAND's capacity for cross-context transfer by testing on completely unseen cell-line contexts. This is challenging as cell lines from different lineages (e.g., myeloid K562 vs. epithelial RPE1) exhibit substantial covariate shift in both

Table 2. Gene perturbation performance comparison. Results are reported for *single cell-line evaluation*: models are trained and evaluated *independently* on each cell line (K562, Jurkat, RPE1), and metrics are averaged across cell lines under the low-sample and zero-shot settings. Detailed per-cell-line results are reported in Table S5 (low-sample), Table S6 (zero-shot, full gene set), and Table S7 (zero-shot subset with GEARS).

Task	Method	Distributional Fidelity		DE Signal		Global Fit		Summary
		Discr. Cos \uparrow	E-Dist \downarrow	Dir. Match \uparrow	Prec. @N \uparrow	Ov. @N \uparrow	Δ Pearson \uparrow	
Low-sample	BioLord	5.04 \pm 0.09	9.41 \pm 0.11	6.10 \pm 0.04	0.72 \pm 0.02	0.40 \pm 0.02	0.16 \pm 0.00	1.38 \pm 0.04
	GEARS	5.40 \pm 0.10	1.64 \pm 0.06	7.05 \pm 0.05	0.71 \pm 0.02	0.77 \pm 0.03	0.31 \pm 0.01	1.19 \pm 0.03
	Linear	5.04 \pm 0.09	8.90 \pm 0.08	3.91 \pm 0.03	1.00 \pm 0.04	1.03 \pm 0.03	0.19 \pm 0.01	1.11 \pm 0.03
	PerturbMean	5.02 \pm 0.09	8.91 \pm 0.08	8.43 \pm 0.03	0.22 \pm 0.01	0.58 \pm 0.02	0.52 \pm 0.01	1.03 \pm 0.03
	STATE	6.40 \pm 0.09	12.46 \pm 0.11	5.75 \pm 0.06	0.74 \pm 0.02	0.38 \pm 0.02	0.13 \pm 0.01	5.06 \pm 0.09
Zero-shot	STRAND	7.10 \pm 0.09	2.07 \pm 0.05	7.69 \pm 0.05	0.74 \pm 0.02	1.21 \pm 0.04	0.39 \pm 0.01	1.04 \pm 0.03
	BioLord	5.05 \pm 0.09	9.44 \pm 0.11	6.15 \pm 0.04	0.77 \pm 0.02	0.45 \pm 0.02	0.15 \pm 0.00	1.30 \pm 0.04
	Linear	5.03 \pm 0.09	8.91 \pm 0.08	3.83 \pm 0.03	1.00 \pm 0.04	1.02 \pm 0.03	0.20 \pm 0.01	1.04 \pm 0.03
	PerturbMean	5.02 \pm 0.09	8.92 \pm 0.08	8.43 \pm 0.03	0.22 \pm 0.01	0.58 \pm 0.02	0.52 \pm 0.01	1.03 \pm 0.03
	STATE	N/A	N/A	N/A	N/A	N/A	N/A	N/A
	STRAND	5.17 \pm 0.09	2.38 \pm 0.07	7.25 \pm 0.05	0.78 \pm 0.02	1.15 \pm 0.04	0.34 \pm 0.01	1.10 \pm 0.03

gene expression patterns and regulatory architectures.

We conduct leave-one-cell-line-out evaluation using the *Combined* dataset, training on two cell lines and testing on the third. We evaluate the 300 most prevalent perturbations in each hold-out cell line across all contexts to ensure consistent comparison. As shown in Figure S1, STATE achieves performance that is only marginally better than the *Identity* baseline (simply predicting control expression) across all three holdout scenarios. In contrast, STRAND is more robust in learning biologically relevant signal from the limited cellular context exposed, outperforms STATE and baseline across all transfer tasks, achieving improvements of Δ Pearson $r \approx 0.14$ on K562 transfer on average, compared to STATE, and consistently outperforms the *Identity* baseline, with an improvement of top gene direction match by $> 10\%$. We hypothesize this advantage stems from STRAND’s sequence-level modeling, which effectively learns the generalizable context-dependent regulatory logic through the mechanistically grounded inductive bias.

5.2. Ablation Studies

To isolate the contributions of our key architectural components, specifically the DNA Perturbation Module and the Latent Diffusion Module, we conducted the following ablation analyses.

DNA Perturbation Module. We hypothesize that co-training with the perturbation module improves the model ability to retrieve the finer interventional relationship between regulatory activation and transcriptional response from the pretrained DNA embeddings. To verify this, we compared our full model against a baseline where the perturbation module is replaced by average-pooled, fixed DNA embeddings (termed **w/o Perturb Module**). Using the low-sample setting, we computed the Pearson correlation and proportion of directional match between the predicted and ground-truth expression changes $\Delta(\mathbf{x}_p - \mathbf{x}_c)$ for the top-

K most differentially expressed genes. Figure 4 illustrates the performance difference across K . The module-based model shows an average of 12.08% improvement in Pearson correlation and 11.39% improvement in effect direction match over the fixed baseline. This confirms that learning perturbation-specific embeddings is important for prioritizing significant biological effects.

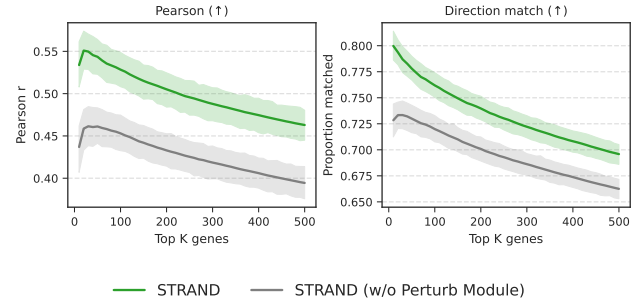


Figure 4. Ablation of the STRAND DNA Perturbation Module. Models are trained on the *Combined* dataset. Plots show statistics for the top- K genes with the largest absolute expression changes. Shaded regions denote 95% CIs.

Generative Transport vs. Predictive Fusion. To isolate gains from distributional modeling, we evaluate a concatenation baseline that replaces stochastic transport with deterministic MLP prediction on $[\mathbf{z}_c; \mathbf{z}^{\text{DNA}}]$, using identical encoders, decoder, and losses (except diffusion), so the only change is pointwise regression versus distributional transport. As shown in Figure 5, the generative model reduces E-Distance by 38.9% and increases R^2 by 27.6% on the combined dataset. Further ablation on CLIP loss is reported in Table S8.

5.3. Sequence-Resolved In Silico Perturbation Profiling (Hypothesis Generation)

STRAND conditions directly on DNA sequence, enabling virtual perturbation screening at arbitrary genomic coor-

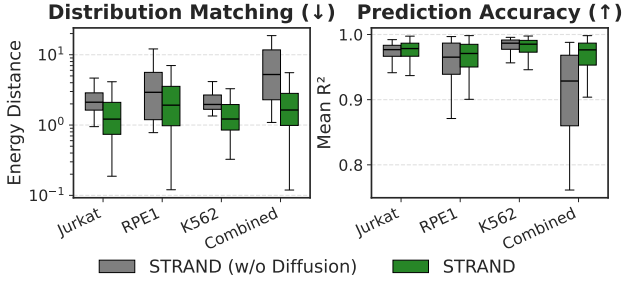


Figure 5. Ablation of the STRAND RNA Generative Transport
Generative model demonstrates better fidelity in modeling the distribution

dinates and discrimination among alternative regulatory elements within a gene. We validate this by (i) prioritizing alternative TSSs with known functional differences and (ii) recovering cell-type-specific regulatory landscapes at lineage-defining genes.

We slide a 100 bp perturbation window and compute E-distance between predicted perturbed and control expression, producing sequence-level perturbation impact profiles. These recover known regulatory landmarks and highlight candidate segments for follow-up. For each site, we use 64 control cells, estimate uncertainty via 20 bootstraps, and apply Gaussian smoothing.

Alternative TSS Discovery. Genes initiate transcription at transcription start sites (TSSs). When multiple TSSs exist for a gene, perturbation designs and gene-level models typically focus on the canonical site, even though alternative TSSs can be functionally dominant.

We examined *FLVCR1* in K562 cells, which uses alternative TSSs to produce two distinct isoforms. *FLVCR1a*, transcribed from the canonical TSS, localizes to the plasma membrane and functions as a heme exporter. In contrast, *FLVCR1b* is transcribed from an alternative TSS within the first intron and produces a mitochondrial heme exporter required for erythroid differentiation (Chiabrandi et al., 2012). Experimental studies show that *FLVCR1b*, rather than *FLVCR1a*, drives hemoglobinization and erythroid differentiation in K562 cells. Silencing *FLVCR1b* blocks differentiation (Chiabrandi et al., 2012).

Our *in silico* perturbations ranked the *FLVCR1b* TSS (FLVCR1-202, chr1:212,859,916) highest among all of the five *FLVCR1* transcripts (E-dist = 0.683), exceeding the canonical *FLVCR1a* TSS (E-dist = 0.564; Table S9). The functional importance of the alternative *FLVCR1b* promoter in K562 cells is a distinction that gene-level models (GEARS, BioLord, STATE) cannot capture.

In Silico Screening. We examine three representative gene-cell-line pairs with well-characterized cell-type-specific functions.

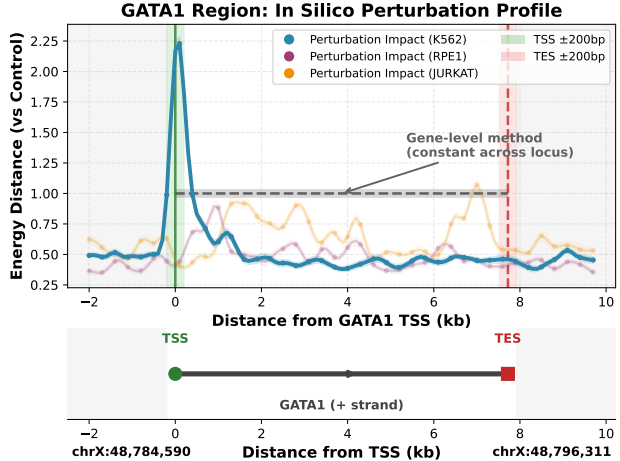


Figure 6. Virtual perturbation screening at the *GATA1* locus.
STRAND captures the cell-type specific sensitivity of *GATA1* in **K562** cells, precisely locating the peak impact at the TSS, while ignoring non-expressing lines (Jurkat, RPE1). Gene-level methods (gray) cannot capture the variation and is confined at gene region.

***GATA1* in K562 cells:** *GATA1* is a master transcription factor essential for erythroid differentiation, and K562 is an erythroleukemia cell line where *GATA1* plays a critical regulatory role (Moriguchi & Yamamoto, 2014). STRAND predicts a cell-type-specific response: K562 shows a sharp peak in perturbation sensitivity at the TSS, while RPE1 and Jurkat cells exhibit minimal response throughout the locus (Figure 6). This specificity aligns with *GATA1*'s known lineage-restricted function. Similarly, we demonstrate STRAND's ability to identify two additional cell-line-specific gene activities, *CD3D* in Jurkat (Fig. S2) and *KRT18* in RPE1 (Fig. S3), at the correct sequence locations. Detailed documentation is provided in App. J.2.

6. Conclusion

We introduced STRAND, a sequence-conditioned generative model for predicting single-cell perturbation responses that represents perturbations through regulatory DNA. By combining DNA-derived perturbation embeddings with control-anchored generative transport, STRAND models heterogeneous perturbation effects at nucleotide resolution. Across low-sample, zero-shot, and cross-cell-line evaluations, STRAND consistently outperforms state-of-the-art gene-level methods and achieves the best overall rank across seven evaluation metrics. STRAND enables accurate sequence-resolved *in silico* perturbation profiling and recovers functional regulatory elements that are inaccessible to existing models. These results establish STRAND as a unified framework for linking genomic sequence to population-level transcriptional responses. Limitations and future directions are discussed in App. K.

Acknowledgment

We thank Ruthie Johnson, Nanxiang Zhao, Yepeng Huang, and Intae Moon for their helpful feedback. We thank Peter Halmos for his feedback on experimental design. B.F., X.L., and M.Z. gratefully acknowledge the support of the Merck Award. Sa.G. was supported by the Dr. Susanne E. Churchill Summer Institute in Biomedical Informatics (SIBMI) at Harvard Medical School. B.F., Sa.G., X.L., Sh.G., X.S., and M.Z. were additionally supported, in part, by NSF CAREER Award 2339524, ARPA-H Biomedical Data Fabric (BDF) Toolbox Program, Amazon Faculty Research, Google Research Scholar Program, AstraZeneca Research, GlaxoSmithKline Award, Roche Alliance with Distinguished Scientists (ROADS) Program, Sanofi iDEA-iTECH Award, Boehringer Ingelheim Award, Optum AI Research Collaboration Award, Pfizer Research, Gates Foundation (INV-079038), Chan Zuckerberg Initiative, John and Virginia Kaneb Fellowship at Harvard Medical School, Biswas Computational Biology Initiative in partnership with the Milken Institute, Harvard Medical School Dean's Innovation Fund for the Use of Artificial Intelligence, and the Kempner Institute for the Study of Natural and Artificial Intelligence at Harvard University. Any opinions, findings, conclusions, or recommendations expressed in this material are those of the authors and do not necessarily reflect the views of the funders.

Broader Impact

This work advances machine learning methods for modeling genetic perturbation effects by introducing sequence-conditioned generative transport for single-cell transcriptomics. By enabling nucleotide-resolution prediction of perturbation responses, the proposed framework may support hypothesis generation in functional genomics, guide experimental design, and improve interpretation of non-coding genetic variation relevant to human disease.

The model is intended for in silico analysis and does not directly enable genome editing or clinical intervention. However, as with many computational methods in genomics, downstream applications could influence experimental prioritization in biomedical research. Misinterpretation of model predictions without experimental validation could lead to incorrect biological conclusions. We therefore emphasize that STRAND is designed as a predictive and exploratory tool rather than a substitute for empirical experimentation.

The datasets used are publicly available and de-identified, and the work does not introduce new privacy risks. We do not foresee immediate negative societal impacts beyond those already associated with the broader use of machine learning in biological research. Overall, this work contributes methodological advances to machine learning with

potential positive impact on biological discovery, while raising no ethical concerns beyond standard considerations for computational genomics research.

References

Adduri, A. K., Gautam, D., Bevilacqua, B., Imran, A., Shah, R., Naghipourfar, M., Teyssier, N., Ilango, R., Nagaraj, S., Dong, M., Ricci-Tam, C., Carpenter, C., Subramanyam, V., Winters, A., Tirukkovaular, S., Sullivan, J., Plosky, B. S., Eraslan, B., Youngblut, N. D., Leskovec, J., Gilbert, L. A., Konermann, S., Hsu, P. D., Dobin, A., Burke, D. P., Goodarzi, H., and Roohani, Y. H. Predicting cellular responses to perturbation across diverse contexts with state. June 2025a. doi: 10.1101/2025.06.26.661135. URL <http://dx.doi.org/10.1101/2025.06.26.661135>.

Adduri, A. K., Gautam, D., Bevilacqua, B., Imran, A., Shah, R., Naghipourfar, M., Teyssier, N., Ilango, R., Nagaraj, S., Dong, M., et al. Predicting cellular responses to perturbation across diverse contexts with state. *BioRxiv*, pp. 2025–06, 2025b.

Ahlmann-Eltze, C., Huber, W., and Anders, S. Deep-learning-based gene perturbation effect prediction does not yet outperform simple linear baselines. *Nature Methods*, 22(8):1657–1661, 2025.

Alarcon, B., Ley, S., Sanchez-Madrid, F., Blumberg, R., Ju, S., Fresno, M., and Terhorst, C. The cd3-gamma and cd3-delta subunits of the t cell antigen receptor can be expressed within distinct functional tcr/cd3 complexes. *The EMBO Journal*, 10(4):903–912, 1991.

Avsec, Ž., Agarwal, V., Visentin, D., Ledsam, J. R., Grabska-Barwinska, A., Taylor, K. R., Assael, Y., Jumper, J., Kohli, P., and Kelley, D. R. Effective gene expression prediction from sequence by integrating long-range interactions. *Nature methods*, 18(10):1196–1203, 2021.

Avsec, Ž., Latysheva, N., Cheng, J., Novati, G., Taylor, K. R., Ward, T., Bycroft, C., Nicolaisen, L., Arvaniti, E., Pan, J., et al. Alphagenome: advancing regulatory variant effect prediction with a unified dna sequence model. *Nature*, pp. 2025–06, 2026.

Bai, D., Song, L., and Xing, E. Pertadapt: Unlocking single-cell foundation models for genetic perturbation prediction via condition-sensitive adaptation. *bioRxiv*, pp. 2025–11, 2025.

Bereket, M. and Karaletsos, T. Modelling cellular perturbations with the sparse additive mechanism shift variational autoencoder. *Advances in Neural Information Processing Systems*, 36:1–12, 2023.

Bunne, C., Stark, S. G., Gut, G., del Castillo, J. S., Levesque, M., Lehmann, K.-V., Pelkmans, L., Krause, A., and Rätsch, G. Learning single-cell perturbation responses using neural optimal transport. *Nature Methods*, 20(11):1759–1768, September 2023. ISSN 1548-7105. doi: 10.1038/s41592-023-01969-x. URL <http://dx.doi.org/10.1038/s41592-023-01969-x>.

Canver, M. C., Smith, E. C., Sher, F., Pinello, L., Sanjana, N. E., Shalem, O., Chen, D. D., Schupp, P. G., Vinjamur, D. S., Garcia, S. P., et al. Bcl11a enhancer dissection by cas9-mediated in situ saturating mutagenesis. *Nature*, 527(7577):192–197, 2015.

Cheng, W., Song, Z., Zhang, Y., Wang, S., Wang, D., Yang, M., Li, L., and Ma, J. Dnalongbench: a benchmark suite for long-range dna prediction tasks. *bioRxiv*, 2025.

Chiabrandi, D., Marro, S., Mercurio, S., Giorgi, C., Petrillo, S., Vinchi, F., Fiorito, V., Fagoonee, S., Camporeale, A., Turco, E., et al. The mitochondrial heme exporter flvcr1b mediates erythroid differentiation. *The Journal of clinical investigation*, 122(12):4569–4579, 2012.

Cui, H., Wang, C., Maan, H., Pang, K., Luo, F., Duan, N., and Wang, B. scgpt: toward building a foundation model for single-cell multi-omics using generative ai. *Nature methods*, 21(8):1470–1480, 2024.

Dong, M., Wang, B., Wei, J., de O. Fonseca, A. H., Perry, C. J., Frey, A., Ouerghi, F., Foxman, E. F., Ishizuka, J. J., Dhodapkar, R. M., et al. Causal identification of single-cell experimental perturbation effects with cinema-ot. *Nature methods*, 20(11):1769–1779, 2023.

Dong, M., Adduri, A., Gautam, D., Carpenter, C., Shah, R., Ricci-Tam, C., Kluger, Y., Burke, D. P., and Roohani, Y. H. Stack: In-context learning of single-cell biology. *bioRxiv*, pp. 2026–01, 2026.

Driessen, A., Harsanyi, B., Rapsomaniki, M., and Born, J. Towards generalizable single-cell perturbation modeling via the conditional monge gap. *arXiv preprint arXiv:2504.08328*, 2025.

Frangoul, H., Altshuler, D., Cappellini, M. D., Chen, Y.-S., Domm, J., Eustace, B. K., Foell, J., de la Fuente, J., Grupp, S., Handgretinger, R., et al. Crispr-cas9 gene editing for sickle cell disease and β -thalassemia. *New England Journal of Medicine*, 384(3):252–260, 2021.

Fu, B., Pazokitoroudi, A., Sudarshan, M., Liu, Z., Subramanian, L., and Sankararaman, S. Fast kernel-based association testing of non-linear genetic effects for biobank-scale data. *Nature communications*, 14(1):4936, 2023.

Garau-Luis, J. J., Bordes, P., Gonzalez, L., Roller, M., de Almeida, B., Blum, C., Hexemer, L., Laurent, S., Lang, M., Pierrot, T., et al. Multi-modal transfer learning between biological foundation models. *Advances in Neural Information Processing Systems*, 37:78431–78450, 2024.

Gaudelet, T., Del Vecchio, A., Carrami, E. M., Cudini, J., Kapourani, C.-A., Uhler, C., and Edwards, L. Season combinatorial intervention predictions with salt & peper. *arXiv preprint arXiv:2404.16907*, 2024.

Gonzalez, G., Lin, X., Herath, I., Veselkov, K., Bronstein, M., and Zitnik, M. Combinatorial prediction of therapeutic perturbations using causally-inspired neural networks. *Nature Biomedical Engineering*, pp. 2025, 2025.

Guo, Z., Liu, J., Wang, Y., Chen, M., Wang, D., Xu, D., and Cheng, J. Diffusion models in bioinformatics and computational biology. *Nature Reviews Bioengineering*, 2(2):136–154, October 2023. ISSN 2731-6092. doi: 10.1038/s44222-023-00114-9. URL <http://dx.doi.org/10.1038/s44222-023-00114-9>.

Halmos, P., Gold, J., Liu, X., and Raphael, B. J. Hierarchical refinement: Optimal transport to infinity and beyond. *arXiv preprint arXiv:2503.03025*, 2025.

Hao, M., Gong, J., Zeng, X., Liu, C., Guo, Y., Cheng, X., Wang, T., Ma, J., Zhang, X., and Song, L. Large-scale foundation model on single-cell transcriptomics. *Nature methods*, 21(8):1481–1491, 2024.

He, S., Zhu, Y., Tavakol, D. N., Ye, H., Lao, Y.-H., Zhu, Z., Xu, C., Chauhan, S., Garty, G., Tomer, R., Vunjak-Novakovic, G., Zou, J., Azizi, E., and Leong, K. W. Squidiff: predicting cellular development and responses to perturbations using a diffusion model. *Nature Methods*, November 2025a. ISSN 1548-7105. doi: 10.1038/s41592-025-02877-y. URL <http://dx.doi.org/10.1038/s41592-025-02877-y>.

He, S., Zhu, Y., Tavakol, D. N., Ye, H., Lao, Y.-H., Zhu, Z., Xu, C., Chauhan, S., Garty, G., Tomer, R., et al. Squidiff: predicting cellular development and responses to perturbations using a diffusion model. *Nature Methods*, pp. 1–13, 2025b.

Heimberg, G., Kuo, T., DePianto, D. J., Salem, O., Heigl, T., Diamant, N., Scalia, G., Biancalani, T., Turley, S. J., Rock, J. R., et al. A cell atlas foundation model for scalable search of similar human cells. *Nature*, 638(8052):1085–1094, 2025.

Hetzel, L., Böhm, S., Kilbertus, N., Günnemann, S., Lotfollahi, M., and Theis, F. J. Predicting cellular responses to novel drug perturbations at a single-cell resolution. In *NeurIPS 2022*, 2022.

Hingerl, J. C., Karollus, A., and Gagneur, J. Flashzoi: an enhanced borzoi for accelerated genomic analysis. *Bioinformatics*, 41(9):btaf467, 2025.

Huang, A. C., Hsieh, T.-H. S., Zhu, J., Michuda, J., Teng, A., Kim, S., Rumsey, E. M., Lam, S. K., Anigbogu, I., Wright, P., et al. X-atlas/orion: Genome-wide perturb-seq datasets via a scalable fix-cryopreserve platform for training dose-dependent biological foundation models. *bioRxiv*, pp. 2025–06, 2025.

Hunt, R. C. and Davis, A. A. Altered expression of keratin and vimentin in human retinal pigment epithelial cells in vivo and in vitro. *Journal of cellular physiology*, 145(2): 187–199, 1990.

Istrate, A.-M., Milletari, F., Castrotorres, F., Tomczak, J. M., Torkar, M., Li, D., and Karaletsos, T. rbio1-training scientific reasoning llms with biological world models as soft verifiers. *bioRxiv*, pp. 2025–08, 2025.

Kamimoto, K., Stringa, B., Hoffmann, C. M., Jindal, K., Solnica-Krezel, L., and Morris, S. A. Dissecting cell identity via network inference and in silico gene perturbation. *Nature*, 614(7949):742–751, February 2023. ISSN 1476-4687. doi: 10.1038/s41586-022-05688-9. URL <http://dx.doi.org/10.1038/s41586-022-05688-9>.

Kendall, A., Gal, Y., and Cipolla, R. Multi-task learning using uncertainty to weigh losses for scene geometry and semantics. In *Proceedings of the IEEE conference on computer vision and pattern recognition*, pp. 7482–7491, 2018.

Klein, D., Fleck, J. S., Bobrovskiy, D., Zimmermann, L., Becker, S., Palma, A., Dony, L., Tejada-Lapuerta, A., Huguet, G., Lin, H.-C., et al. Cellflow enables generative single-cell phenotype modeling with flow matching. *bioRxiv*, pp. 2025–04, 2025.

Lal, A., Karollus, A., Gunsalus, L., Garfield, D., Nair, S., Tseng, A. M., Gordon, M. G., Blischak, J., van de Geijn, B., Bhangale, T., et al. Decoding sequence determinants of gene expression in diverse cellular and disease states. *bioRxiv*, pp. 2024–10, 2024.

Langley, P. Crafting papers on machine learning. In Langley, P. (ed.), *Proceedings of the 17th International Conference on Machine Learning (ICML 2000)*, pp. 1207–1216, Stanford, CA, 2000. Morgan Kaufmann.

Liang, Z., Zhuang, S., Jiao, X., Mao, W., Chen, H., and Shen, C. scppdm: A diffusion model for single-cell drug-response prediction. *arXiv preprint arXiv:2510.11726*, 2025.

Linder, J., Yuan, H., and Kelley, D. R. Predicting cell type-specific coverage profiles from dna sequence. *bioRxiv*, pp. 2025–06, 2025.

Liu, G.-H., Vahdat, A., Huang, D.-A., Theodorou, E. A., Nie, W., and Anandkumar, A. I^2 sb: Image-to-image schrödinger bridge. *arXiv preprint arXiv:2302.05872*, 2023a.

Liu, G.-H., Vahdat, A., Huang, D.-A., Theodorou, E. A., Nie, W., and Anandkumar, A. I\$^2\$SB: Image-to-Image Schrödinger Bridge, May 2023b. URL <http://arxiv.org/abs/2302.05872>. arXiv:2302.05872 [cs].

Liu, H. and Jin, S. Learning cross-domain representations for transferable drug perturbations on single-cell transcriptional responses. In *Proceedings of the AAAI Conference on Artificial Intelligence*, volume 39, pp. 18834–18842, 2025.

Lorch, L., Zhang, J., Bunne, C., Krause, A., Schölkopf, B., and Uhler, C. Latent causal diffusions for single-cell perturbation modeling. *arXiv preprint arXiv:2601.15341*, 2026.

Lotfollahi, M., Wolf, F. A., and Theis, F. J. scgen predicts single-cell perturbation responses. *Nature Methods*, 16(8):715–721, July 2019. ISSN 1548-7105. doi: 10.1038/s41592-019-0494-8. URL <http://dx.doi.org/10.1038/s41592-019-0494-8>.

Lotfollahi, M., Klimovskaia Susmelj, A., De Donno, C., Hetzel, L., Ji, Y., Ibarra, I. L., Srivatsan, S. R., Naghipourfar, M., Daza, R. M., Martin, B., Shendure, J., McFaleine-Figueroa, J. L., Boyeau, P., Wolf, F. A., Yakubova, N., Günemann, S., Trapnell, C., Lopez-Paz, D., and Theis, F. J. Predicting cellular responses to complex perturbations in high-throughput screens. *Molecular Systems Biology*, 19(6), May 2023a. ISSN 1744-4292. doi: 10.1525/msb.202211517. URL <http://dx.doi.org/10.1525/msb.202211517>.

Lotfollahi, M., Klimovskaia Susmelj, A., De Donno, C., Hetzel, L., Ji, Y., Ibarra, I. L., Srivatsan, S. R., Naghipourfar, M., Daza, R. M., Martin, B., et al. Predicting cellular responses to complex perturbations in high-throughput screens. *Molecular Systems Biology*, pp. e11517, 2023b.

Luecken, M. D., Büttner, M., Chaichoompu, K., Danese, A., Interlandi, M., Mueller, M. F., Strobl, D. C., Zapria, L., Dugas, M., Colomé-Tatché, M., and Theis, F. J. Benchmarking atlas-level data integration in single-cell genomics. *Nature Methods*, 19(1):41–50, December 2021. ISSN 1548-7105. doi: 10.1038/s41592-021-01336-8. URL <http://dx.doi.org/10.1038/s41592-021-01336-8>.

Luo, E., Hao, M., Wei, L., and Zhang, X. scdiffusion: conditional generation of high-quality single-cell data using diffusion model. *Bioinformatics*, 40(9), August 2024. ISSN 1367-4811. doi: 10.1093/bioinformatics/btae518. URL <http://dx.doi.org/10.1093/bioinformatics/btae518>.

Maurano, M. T., Humbert, R., Rynes, E., Thurman, R. E., Haugen, E., Wang, H., Reynolds, A. P., Sandstrom, R., Qu, H., Brody, J., et al. Systematic localization of common disease-associated variation in regulatory dna. *Science*, 337(6099):1190–1195, 2012.

Moriguchi, T. and Yamamoto, M. A regulatory network governing gata1 and gata2 gene transcription orchestrates erythroid lineage differentiation. *International journal of hematology*, 100(5):417–424, 2014.

Murphy, A. E., Fancy, N., and Skene, N. Avoiding false discoveries in single-cell rna-seq by revisiting the first alzheimer's disease dataset. *Elife*, 12:RP90214, 2023.

Nadig, A., Reppogle, J. M., Pogson, A. N., Murthy, M., McCarroll, S. A., Weissman, J. S., Robinson, E. B., and O'Connor, L. J. Transcriptome-wide analysis of differential expression in perturbation atlases. *Nature Genetics*, pp. 1–10, 2025.

Nasser, J., Bergman, D. T., Fulco, C. P., Guckelberger, P., Doughty, B. R., Patwardhan, T. A., Jones, T. R., Nguyen, T. H., Ulirsch, J. C., Lekschas, F., et al. Genome-wide enhancer maps link risk variants to disease genes. *Nature*, 593(7858):238–243, 2021.

Pampari, A., Shcherbina, A., Kvon, E. Z., Kosicki, M., Nair, S., Kundu, S., Kathiria, A. S., Risca, V. I., Kuningas, K., Alasoo, K., et al. Chrombpnet: bias factorized, base-resolution deep learning models of chromatin accessibility reveal cis-regulatory sequence syntax, transcription factor footprints and regulatory variants. *BioRxiv*, pp. 2024–12, 2025.

Park, K. and Li, H. Causal network recovery in perturb-seq experiments using proxy and instrumental variables. *arXiv preprint arXiv:2601.01830*, 2026.

Passigan, P., Ning, A., et al. Interpretable perturbation modeling through biomedical knowledge graphs. *arXiv preprint arXiv:2512.22251*, 2025.

Patel, A., Singhal, A., Wang, A., Pampari, A., Kasowski, M., and Kundaje, A. Dart-eval: A comprehensive dna language model evaluation benchmark on regulatory dna. *Advances in Neural Information Processing Systems*, 37: 62024–62061, 2024.

Peidli, S., Green, T. D., Shen, C., Gross, T., Min, J., Garda, S., Yuan, B., Schumacher, L. J., Taylor-King, J. P., Marks, D. S., Luna, A., Blüthgen, N., and Sander, C. scperturb: harmonized single-cell perturbation data. *Nature Methods*, 21(3):531–540, January 2024. ISSN 1548-7105. doi: 10.1038/s41592-023-02144-y. URL <http://dx.doi.org/10.1038/s41592-023-02144-y>.

Piran, Z., Cohen, N., Hoshen, Y., and Nitzan, M. Disentanglement of single-cell data with biolord. *Nature Biotechnology*, 42(11):1678–1683, January 2024. ISSN 1546-1696. doi: 10.1038/s41587-023-02079-x. URL <http://dx.doi.org/10.1038/s41587-023-02079-x>.

Radford, A., Kim, J. W., Hallacy, C., Ramesh, A., Goh, G., Agarwal, S., Sastry, G., Askell, A., Mishkin, P., Clark, J., et al. Learning transferable visual models from natural language supervision. In *International conference on machine learning*, pp. 8748–8763. PMLR, 2021.

Roohani, Y., Huang, K., and Leskovec, J. Predicting transcriptional outcomes of novel multigene perturbations with gears. *Nature Biotechnology*, 42(6): 927–935, August 2023. ISSN 1546-1696. doi: 10.1038/s41587-023-01905-6. URL <http://dx.doi.org/10.1038/s41587-023-01905-6>.

Smith, C. C., Paguirigan, A., Jeschke, G. R., Lin, K. C., Massi, E., Tarver, T., Chin, C.-S., Asthana, S., Olshen, A., Travers, K. J., et al. Heterogeneous resistance to quizartinib in acute myeloid leukemia revealed by single-cell analysis. *Blood, The Journal of the American Society of Hematology*, 130(1):48–58, 2017.

Song, B., Liu, D., Dai, W., McMyn, N. F., Wang, Q., Yang, D., Krejci, A., Vasilyev, A., Untermoser, N., Loregger, A., et al. Decoding heterogeneous single-cell perturbation responses. *Nature cell biology*, pp. 1–12, 2025.

Squair, J. W., Gautier, M., Kathe, C., Anderson, M. A., James, N. D., Hutson, T. H., Hudelle, R., Qaiser, T., Matson, K. J., Barraud, Q., et al. Confronting false discoveries in single-cell differential expression. *Nature communications*, 12(1):5692, 2021.

Szałata, A., Benz, A., Cannoodt, R., Cortes, M., Fong, J., Kuppasani, S., Lieberman, R., Liu, T., Mas-Rosario, J. A., Meinl, R., et al. A benchmark for prediction of transcriptomic responses to chemical perturbations across cell types. *Advances in Neural Information Processing Systems*, 37:20566–20616, 2024.

Theodoris, C. V., Xiao, L., Chopra, A., Chaffin, M. D., Al Sayed, Z. R., Hill, M. C., Mantineo, H., Brydon, E. M., Zeng, Z., Liu, X. S., et al. Transfer learning enables predictions in network biology. *Nature*, 618(7965):616–624, 2023.

Tong, A., Huang, J., Wolf, G., Van Dijk, D., and Krishnaswamy, S. Trajectorynet: a dynamic optimal transport network for modeling cellular dynamics. In *Proceedings of the 37th International Conference on Machine Learning*, ICML'20. JMLR.org, 2020.

Tu, X., Hütter, J.-C., Wang, Z. J., Kudo, T., Regev, A., and Lopez, R. A supervised contrastive framework for learning disentangled representations of cellular perturbation data. In *Machine Learning in Computational Biology*, pp. 90–100. PMLR, 2024.

Viñas Torné, R., Wiatrak, M., Piran, Z., Fan, S., Jiang, L., Teichmann, S. A., Nitzan, M., and Brbić, M. Systema: a framework for evaluating genetic perturbation response prediction beyond systematic variation. *Nature Biotechnology*, pp. 1–10, 2025.

Wang, C., Gupta, S., Uhler, C., and Jaakkola, T. Removing biases from molecular representations via information maximization. *arXiv preprint arXiv:2312.00718*, 2023.

Wei, J., Xue, Y., Chai, H., and Gao, Y. Q. Genome: a moe-based generative model for individualized, multimodal prediction and perturbation of genomic profiles. *bioRxiv*, pp. 2025–12, 2025.

Wenkel, F., Tu, W., Masschelein, C., Shirzad, H., Eastwood, C., Whitfield, S. T., Bendidi, I., Russell, C., Hodgson, L., Mesbahi, Y. E., et al. Txpert: Leveraging biochemical relationships for out-of-distribution transcriptomic perturbation prediction. *arXiv preprint arXiv:2505.14919*, 2025.

Wu, M., Littman, R., Levine, J., Qiu, L., Biancalani, T., Richmond, D., and Huetter, J.-C. Contextualizing biological perturbation experiments through language. *arXiv preprint arXiv:2502.21290*, 2025.

Wu, Y., Barton, R. A., Wang, Z., Ioannidis, V. N., De Donno, C., Price, L. C., Voloch, L. F., and Karypis, G. Predicting cellular responses with variational causal inference and refined relational information. *arXiv preprint arXiv:2210.00116*, 2022.

Wu, Y., Wershof, E., Schmon, S. M., Nassar, M., Osiński, B., Eksi, R., Yan, Z., Stark, R., Zhang, K., and Graepel, T. Perturbbench: Benchmarking machine learning models for cellular perturbation analysis. *arXiv preprint arXiv:2408.10609*, 2024.

Yu, H., Qian, W., Song, Y., and Welch, J. D. Perturbnet predicts single-cell responses to unseen chemical and genetic perturbations. *Molecular Systems Biology*, 21(8): 960, 2025.

Zhu, O. and Li, J. Scouter predicts transcriptional responses to genetic perturbations with large language model embeddings. *Nature Computational Science*, pp. 1–8, 2025.

A. Optimal Transport Coupling Details

STRAND can flexibly adapt different OT pairing algorithms. By default, we employ Hierarchical Refinement Optimal Transport (HiRef) (Halmos et al., 2025) to compute bijective couplings between control and perturbed cell populations. Below, we detail the complete OT protocol, including the cost function, solver, hyperparameters, and preprocessing steps.

A.1. Embedding and Latent Space Representation

Cell Embeddings. We represent each cell using SCimilarity embeddings (Nadig et al., 2025), a pre-trained foundation model that maps gene expression profiles to a 128-dimensional latent space. Let $\mathbf{e}_i \in \mathbb{R}^{128}$ denote the embedding for cell i .

Dimensionality Reduction. For each perturbation-control matching task, we apply Principal Component Analysis (PCA) to the combined embeddings of control and perturbed cells. Let $\mathcal{C} = \{\mathbf{e}_1^c, \dots, \mathbf{e}_n^c\}$ and $\mathcal{P} = \{\mathbf{e}_1^p, \dots, \mathbf{e}_m^p\}$ denote the control and perturbed cell embeddings, respectively. We compute:

$$\mathbf{Z}_{\text{combined}} = [\mathcal{C}; \mathcal{P}] \in \mathbb{R}^{(n+m) \times 128} \quad (\text{S1})$$

and apply PCA with $d = \min(50, n + m - 1)$ components to obtain the reduced representations $\mathbf{X}^c \in \mathbb{R}^{n \times d}$ and $\mathbf{X}^p \in \mathbb{R}^{m \times d}$.

A.2. Cost Function

The transport cost between control cell embedding i and perturbed cell embedding j is defined as the squared Euclidean distance in the PCA-reduced latent space:

$$C_{ij} = \|\mathbf{z}_c^i - \mathbf{z}_p^j\|_2^2 \quad (\text{S2})$$

where \mathbf{z}_c^i and \mathbf{z}_p^j are the PCA-transformed embeddings.

A.3. Optimal Transport Solver: Hierarchical Refinement

We use the Hierarchical Refinement (HiRef) algorithm (Halmos et al., 2025), which computes the exact Monge map (bijective coupling) in log-linear time and linear space.

Algorithm Overview. HiRef leverages low-rank OT to iteratively partition both source and target distributions through a hierarchy of subproblems. At each level, the algorithm:

1. Solves a low-rank OT problem to co-cluster source-target pairs
2. Partitions the data according to the cluster assignments
3. Recursively refines each partition until reaching singleton matches

Rank Annealing Schedule. We employ the default optimal rank schedule:

$$\text{rank_schedule} = \text{optimal_rank_schedule}(n, \text{depth} = 6, Q_{\text{max}} = \max(2^{15}, n), r_{\text{max}} = 2^{10}) \quad (\text{S3})$$

where n is the number of cells to match, $\text{depth} = 6$ controls the hierarchy depth, Q_{max} is the maximum subproblem size, and $r_{\text{max}} = 1024$ is the maximum rank at any level.

A.4. Sample Size Handling and Bootstrapping

We employ a “floor without ceiling” strategy for sample size balancing:

Minimum Cell Threshold. We set $n_{\text{min}} = 30$ as the minimum number of cells per perturbation group.

Bootstrapping Protocol. For each perturbation group with n_{pert} cells:

- If $n_{\text{pert}} < n_{\text{min}}$: Bootstrap (sample with replacement) to exactly n_{min} cells
- If $n_{\text{pert}} \geq n_{\text{min}}$: Use all available cells without downsampling

Control Sampling. Controls are sampled (with replacement if necessary) to match the perturbation group size, ensuring 1:1 matching:

$$|\mathcal{C}_{\text{matched}}| = |\mathcal{P}_{\text{matched}}| = \max(n_{\min}, n_{\text{pert}}) \quad (\text{S4})$$

Cell-Line Aware Matching. When cell-line annotations are available, we enforce strict within-cell-line matching:

$$\mathcal{C}_{\text{candidates}} = \{c \in \mathcal{C} : \text{cell_line}(c) = \text{cell_line}(\mathcal{P})\} \quad (\text{S5})$$

A.5. Hyperparameter Summary

Table S1. OT matching hyperparameters

Parameter	Value	Description
PCA components	$\min(50, n - 1)$	Latent space dimensionality
Cost function	Squared Euclidean	Distance metric in PCA space
Hierarchy depth	6	Number of refinement levels
Max rank (r_{\max})	$2^{10} = 1024$	Maximum rank per level
Max subproblem (Q_{\max})	$\max(2^{15}, n)$	Largest subproblem size
Base rank (r_0)	1	Binary partitioning
Min cells (n_{\min})	30	Bootstrap threshold

A.6. Computational Complexity

HiRef achieves $O(n \log n)$ time complexity and $O(n)$ space complexity, compared to $O(n^2)$ time and space for Sinkhorn-based methods. This enables scaling to datasets with millions of cells.

A.7. Sensitivity Analysis

PCA Components. The choice of 50 PCA components captures $> 95\%$ of the variance in SCimilarity embeddings while providing sufficient dimensionality reduction for stable OT computation. We empirically verified that results are robust to choices in the range [30, 100] components.

Bootstrap Threshold. The minimum cell threshold $n_{\min} = 30$ balances statistical power with representation of rare perturbations.

Regularization. Unlike Sinkhorn-based OT which requires tuning the entropic regularization parameter ε , HiRef directly computes the unregularized Monge map, eliminating a source of hyperparameter sensitivity.

A.8. Implementation Details

All OT computations were performed using the HiRef implementation¹ with PyTorch on NVIDIA GPUs. The complete pipeline code is available in our supplementary materials.

B. Derivations for I2SB

B.1. Bridge and forward process (I2SB)

We model perturbation effects in a shared latent space. Let $\mathbf{z}_0 = \mathbf{z}_p \in \mathbb{R}^D$ denote the *perturbed* latent (clean endpoint) and $\mathbf{z}_1 = \mathbf{z}_c \in \mathbb{R}^D$ the *control* latent (degraded endpoint). Following I2SB, we define a Gaussian diffusion *bridge* between $(\mathbf{z}_0, \mathbf{z}_1)$. For discrete steps $t \in \{0, \dots, T\}$, define the cumulative noise

$$\sigma_t^2 \doteq \sum_{n=0}^{t-1} \beta_n, \quad \bar{\sigma}_t^2 \doteq \sigma_T^2 - \sigma_t^2.$$

¹<https://github.com/raphael-group/HiRef>

Then the analytic bridge marginal is

$$q(\mathbf{z}_t \mid \mathbf{z}_0, \mathbf{z}_1) = \mathcal{N}\left(\mathbf{z}_t; w_0(t)\mathbf{z}_0 + w_1(t)\mathbf{z}_1, \sigma^2(t)\mathbf{I}\right), \quad (\text{S6})$$

with weights and variance

$$w_0(t) = \frac{\bar{\sigma}_t^2}{\bar{\sigma}_t^2 + \sigma_t^2}, \quad w_1(t) = \frac{\sigma_t^2}{\bar{\sigma}_t^2 + \sigma_t^2}, \quad \sigma^2(t) = \frac{\sigma_t^2 \bar{\sigma}_t^2}{\bar{\sigma}_t^2 + \sigma_t^2}.$$

Equivalently, we sample $\mathbf{z}_t = w_0(t)\mathbf{z}_0 + w_1(t)\mathbf{z}_1 + \sigma(t)\boldsymbol{\epsilon}$, $\boldsymbol{\epsilon} \sim \mathcal{N}(\mathbf{0}, \mathbf{I})$.

Schedule. We use the symmetric I2SB noise schedule (increase then decrease), i.e., $\{\beta_n\}$ is an ascending segment concatenated with its reverse, so that σ_t^2 peaks near $t \approx T/2$ and shrinks toward both endpoints. No condition-dependent schedule scaling is used.

B.2. Denoising model and training target

Although \mathbf{z}_t is sampled from the bridge marginal $q(\mathbf{z}_t \mid \mathbf{z}_0, \mathbf{z}_1)$, following I2SB we train the network to predict the forward-process noise with respect to the clean endpoint \mathbf{z}_0 . Specifically, we define the training target as

$$\boldsymbol{\varepsilon}^{\text{I2SB}} \doteq \frac{\mathbf{z}_t - \mathbf{z}_0}{\sigma_t}.$$

The denoising objective is

$$\mathcal{L}_{\text{bridge}} = \mathbb{E}_{\mathbf{z}_0, \mathbf{z}_1, t} \left[\left\| \boldsymbol{\varepsilon}_\theta(\mathbf{z}_t, t, \mathbf{u}_p, \mathbf{z}_1) - \boldsymbol{\varepsilon}^{\text{I2SB}} \right\|_2^2 \right],$$

which is equivalent to the I2SB loss formulation.

B.3. Sampling (DDPM-style reverse bridge)

At test time, we start from a noisy control endpoint, e.g.

$$\mathbf{z}_T \sim \mathcal{N}(\mathbf{z}_1, \sigma_T^2 \mathbf{I}),$$

and run DDPM-style reverse steps. Given current \mathbf{z}_n and $\hat{\boldsymbol{\nu}} = \boldsymbol{\varepsilon}_\theta(\mathbf{z}_n, \tilde{t}, \mathbf{c}, \mathbf{z}_1)$, recover the predicted clean endpoint

$$\hat{\mathbf{z}}_0 = \mathbf{z}_n - \sigma_n \hat{\boldsymbol{\nu}}.$$

Then sample \mathbf{z}_{n-1} from the Gaussian posterior $p(\mathbf{z}_{n-1} \mid \hat{\mathbf{z}}_0, \mathbf{z}_n)$ (using the same DDPM recursion as in I2SB), iterating $n = T, \dots, 1$. (Optionally apply classifier-free guidance by mixing conditional/unconditional $\boldsymbol{\varepsilon}_\theta$ outputs.)

B.4. Operational Definition of Perturbation Site

For CRISPR-i style gene perturbations in PerturbQA, we map each targeted gene to its **canonical TSS** and represent the intervention using a **±200 bp window** centered at that TSS. This window is intentionally coarse: it is large enough to cover typical promoter-proximal targeting while remaining local enough to preserve sequence specificity. In future work, STRAND can be extended to incorporate **sgRNA sequence and exact cut/target coordinates** when available, enabling finer modeling of guide-dependent effects.

B.5. Default Inference Configuration

- Samples per perturbation: 256
- Classifier-free guidance scale: 1
- DDPM sampling parameter η : 1

All in silico perturbation screening case studies use a fixed 10-step diffusion sampling to balance computational efficiency and performance.

For benchmark evaluations, the number of diffusion steps is treated as a tunable hyperparameter. We perform a grid search over $\{6, 10, 14, 20, 50\}$ and select the value that minimizes the Energy Distance between predicted and ground-truth perturbation effects on the validation set.

C. Sequence-Expression Alignment

C.1. Objectives

We align a sequence-derived perturbation embedding with the corresponding transcriptional effect using a prototypical (perturbation-level) contrastive objective.

C.2. Setup and Notation

In a minibatch, let $\mathcal{P} = \{1, \dots, P\}$ be the set of unique perturbations. For each perturbation $k \in \mathcal{P}$, let \mathcal{B}_k be the set of matched control-perturbed cell pairs $(\mathbf{z}_{c,i}, \mathbf{z}_{p,i})$ with perturbation label k . Let $\mathbf{u}_{k,i}$ denote the sequence-derived perturbation embedding for pair i .

C.3. Perturbation Prototypes (Pseudo-bulk)

We aggregate single-cell pairs into perturbation-level prototypes:

$$\Delta \bar{\mathbf{z}}_k = \frac{1}{|\mathcal{B}_k|} \sum_{i \in \mathcal{B}_k} (\mathbf{z}_{p,i} - \mathbf{z}_{c,i}), \quad \bar{\mathbf{u}}_k = \frac{1}{|\mathcal{B}_k|} \sum_{i \in \mathcal{B}_k} \mathbf{u}_{k,i}. \quad (\text{S7})$$

Optional weighted prototypes. With per-pair weights w_i ,

$$\Delta \bar{\mathbf{z}}_k = \frac{\sum_{i \in \mathcal{B}_k} w_i (\mathbf{z}_{p,i} - \mathbf{z}_{c,i})}{\sum_{i \in \mathcal{B}_k} w_i}, \quad \bar{\mathbf{u}}_k = \frac{\sum_{i \in \mathcal{B}_k} w_i \mathbf{u}_{k,i}}{\sum_{i \in \mathcal{B}_k} w_i}. \quad (\text{S8})$$

C.4. Asymmetric Projection and Normalization

We project only the DNA prototype to the RNA latent dimension to avoid shifting the pretrained RNA space. Let $\text{Proj}_{\text{DNA}} : \mathbb{R}^{d_{\text{DNA}}} \rightarrow \mathbb{R}^{d_{\text{RNA}}}$ be a 2-layer MLP with GELU:

$$\text{Proj}_{\text{DNA}}(\mathbf{u}) = W_2 \text{GELU}(W_1 \mathbf{u} + b_1) + b_2, \quad (\text{S9})$$

where $W_1 \in \mathbb{R}^{d_h \times d_{\text{DNA}}}$, $W_2 \in \mathbb{R}^{d_{\text{RNA}} \times d_h}$ and $d_h = 128$. We then ℓ_2 -normalize:

$$\hat{\mathbf{u}}_k = \frac{\text{Proj}_{\text{DNA}}(\bar{\mathbf{u}}_k)}{\|\text{Proj}_{\text{DNA}}(\bar{\mathbf{u}}_k)\|_2}, \quad \hat{\mathbf{z}}_k = \frac{\Delta \bar{\mathbf{z}}_k}{\|\Delta \bar{\mathbf{z}}_k\|_2}. \quad (\text{S10})$$

C.5. Soft Targets from RNA Similarity

To reduce false negatives among biologically similar perturbations, we form soft targets from RNA-RNA prototype similarity. Define

$$S_{ij} = \hat{\mathbf{z}}_i^\top \hat{\mathbf{z}}_j, \quad i, j \in \mathcal{P}, \quad (\text{S11})$$

(set $S_{ii} = 1$), and a temperature-softened target distribution

$$T_{ij} = \frac{\exp(S_{ij}/\tau_{\text{soft}})}{\sum_{j' \in \mathcal{P}} \exp(S_{ij'}/\tau_{\text{soft}})}, \quad \tau_{\text{soft}} = 0.1. \quad (\text{S12})$$

C.6. Bidirectional Soft-InfoNCE Loss

We compute cross-modal logits

$$L_{ij} = \tau \hat{\mathbf{u}}_i^\top \hat{\mathbf{z}}_j, \quad \tau = \exp(\theta), \quad (\text{S13})$$

where τ is learnable (initialized from $1/\tau_0$ with $\tau_0 = 0.07$) and clamped to $[5, 33]$. Define row- and column-normalized probabilities:

$$p_{ij}^\rightarrow = \frac{\exp(L_{ij})}{\sum_{j' \in \mathcal{P}} \exp(L_{ij'})}, \quad p_{ij}^\leftarrow = \frac{\exp(L_{ij})}{\sum_{i' \in \mathcal{P}} \exp(L_{i'j})}. \quad (\text{S14})$$

The alignment loss is the average cross-entropy to the soft targets in both directions:

$$\mathcal{L}_{\text{align}} = -\frac{1}{2P} \sum_{i \in \mathcal{P}} \sum_{j \in \mathcal{P}} T_{ij} (\log p_{ij}^\rightarrow + \log p_{ij}^\leftarrow). \quad (\text{S15})$$

C.7. EMA Stabilization and Gradient Flow

To reduce minibatch noise, we maintain an EMA bank of RNA prototypes per global perturbation id g_{id_k} :

$$\Delta \bar{z}_k^{\text{EMA}} \leftarrow \beta \Delta \bar{z}_k^{\text{EMA}} + (1 - \beta) \Delta \bar{z}_k, \quad \beta = 0.9. \quad (\text{S16})$$

When enabled, we use $\Delta \bar{z}_k^{\text{EMA}}$ in place of $\Delta \bar{z}_k$ when forming \hat{z}_k and T_{ij} . By default, we detach RNA targets (`detach_rna=True`) so gradients update only the DNA adaptor/projection and not the (frozen) RNA encoder.

C.8. Hyperparameters

: Table S2 summarizes hyperparameters.

Table S2. Hyperparameters for sequence-expression alignment.

Hyperparameter	Value
DNA projection hidden dim (d_h)	128
Projection output dim (d_{RNA})	varies by RNA encoder
Initial temperature ($1/\tau$)	0.07
Temperature clamp range	[5.0, 33.0]
Soft target temperature (τ_{soft})	0.1
EMA momentum (β)	0.9
Loss weight (λ_{align})	1.0
Detach RNA gradients	True

D. Hurdle truncated-Gaussian residual likelihood

We model nonnegative gene expression using a *hurdle* distribution composed of a point mass at zero and a continuous density for strictly positive values. Let $y_{ij} \geq 0$ denote the observed (log-normalized) expression of gene $j \in \{1, \dots, G\}$ in cell i , and let $x_{ij}^{\text{ref}} \geq 0$ be the decoded control/reference baseline. We define the residual

$$r_{ij} \triangleq y_{ij} - x_{ij}^{\text{ref}}, \quad (\text{S17})$$

and enforce nonnegativity without explicit clamping by modeling r_{ij} with a Normal distribution truncated below at

$$a_{ij} \triangleq -x_{ij}^{\text{ref}}, \quad (\text{S18})$$

so that $r_{ij} \in [a_{ij}, \infty)$ and equivalently $y_{ij} = x_{ij}^{\text{ref}} + r_{ij} \geq 0$.

Hurdle gate. The decoder outputs a Bernoulli logit ℓ_{ij} determining whether a gene is nonzero:

$$p_{ij}^{\text{nz}} \triangleq \Pr(y_{ij} > 0) = \sigma(\ell_{ij}), \quad p_{ij}^0 = 1 - p_{ij}^{\text{nz}}. \quad (\text{S19})$$

Truncated Normal residual model. Conditioned on $y_{ij} > 0$, the residual follows a lower-truncated Normal distribution,

$$r_{ij} \mid (y_{ij} > 0) \sim \text{TN}(\mu_{ij}, \sigma_{ij}^2; a_{ij}, \infty), \quad (\text{S20})$$

with parameters (μ_{ij}, σ_{ij}) predicted by the decoder. Let $\phi(\cdot)$ and $\Phi(\cdot)$ denote the standard Normal pdf and cdf. The truncated density for $r \geq a$ is

$$p_{\text{TN}}(r; \mu, \sigma, a) = \frac{1}{\sigma} \frac{\phi(\frac{r-\mu}{\sigma})}{1 - \Phi(\frac{a-\mu}{\sigma})}. \quad (\text{S21})$$

Defining

$$z_{ij} = \frac{r_{ij} - \mu_{ij}}{\sigma_{ij}}, \quad \alpha_{ij} = \frac{a_{ij} - \mu_{ij}}{\sigma_{ij}}, \quad (\text{S22})$$

the corresponding log-density is

$$\log p_{\text{TN}}(r_{ij}) = \log \phi(z_{ij}) - \log \sigma_{ij} - \log(1 - \Phi(\alpha_{ij})). \quad (\text{S23})$$

Log-likelihood. Combining the hurdle gate and truncated residual model yields

$$\log p(y_{ij} \mid x_{ij}^{\text{ref}}) = \mathbb{I}[y_{ij} = 0] \log p_{ij}^0 + \mathbb{I}[y_{ij} > 0] (\log p_{ij}^{\text{nz}} + \log p_{\text{TN}}(r_{ij})). \quad (\text{S24})$$

Reconstruction objective. We minimize the negative mean log-likelihood over genes and cells:

$$\mathcal{L}_{\text{rec}} = -\frac{1}{|\mathcal{B}|G} \sum_{i \in \mathcal{B}} \sum_{j=1}^G \log p(y_{ij} \mid x_{ij}^{\text{ref}}), \quad (\text{S25})$$

with an optional weighted variant when per-cell weights are provided. A mild variance regularizer $\lambda_\sigma \mathbb{E}[\sigma_{ij}^2]$ is optionally added.

Conditional mean and nonnegativity. For the continuous component, the conditional mean of a lower-truncated Normal satisfies

$$\mathbb{E}[r \mid r \geq a] = \mu + \sigma \lambda(\alpha), \quad \lambda(\alpha) = \frac{\phi(\alpha)}{1 - \Phi(\alpha)}, \quad (\text{S26})$$

where $\lambda(\alpha)$ is the Normal Mills ratio. Consequently,

$$\hat{y}_{ij}^{\text{nz}} = x_{ij}^{\text{ref}} + \mathbb{E}[r_{ij} \mid r_{ij} \geq a_{ij}] \geq 0, \quad (\text{S27})$$

ensuring nonnegative predictions without ad hoc constraints.

E. Model Architecture and Training Details

Model Components. Our architecture integrates four primary components: (i) a DNA encoder/adaptor utilizing Borzoi-derived embeddings; (ii) a conditional diffusion backbone trained with an I2SB/DDPM objective; (iii) a supervised RNA predictor head; and (iv) auxiliary objectives, including CLIP alignment and optional consistency matching.

Notation and Conditioning. Let $x_c, x_p \in \mathbb{R}^{B \times G}$ denote the control and perturbed RNA profiles, respectively, with corresponding latent representations $z_c, z_p \in \mathbb{R}^{B \times d}$ obtained from the pretrained RNA encoder e_ψ . Let $u_p = g_\phi(E_s, m) \in \mathbb{R}^{B \times d_0}$ denote the perturbation embedding produced by the DNA Perturbation Module. We construct the projected DNA condition via a linear transformation followed by Layer Normalization:

$$\Delta c_{\text{diff}} = \text{LN}(W_{\text{diff}} u_p) \in \mathbb{R}^{B \times d_c}. \quad (\text{S28})$$

We also maintain a learned null (cell-line specific) embedding $n_{\text{diff}}(u) \in \mathbb{R}^{d_c}$:

$$c_{\text{diff}}^{\text{null}} = \text{LN}(n_{\text{diff}}(u)) \in \mathbb{R}^{B \times d_c}. \quad (\text{S29})$$

Training Step Regimes. To enable classifier-free guidance and robust conditioning, each training iteration samples one of three conditioning modes for the diffusion condition c_{diff} :

1. **Unconditional Mode (unconditional):** Uses only null embeddings to serve as the unconditional anchor for guidance. To maintain Distributed Data Parallel (DDP) graph connectivity, the DNA projections are retained with a zero multiplier:

$$c_{\text{diff}} = c_{\text{diff}}^{\text{null}}. \quad (\text{S30})$$

2. **Source-Conditional Mode (p_to_p):** Utilizes sequence conditioning with source recentering based on Exponential Moving Average (EMA) statistics. We define the shift $\delta z = \hat{\mu} - \hat{\mu}_c$, where $\hat{\mu}$ denotes the debiased EMA statistics of the respective latents. The source latent is defined as $z_{\text{src}} = z_c + \delta z$. In this mode, only DNA projections are active:

$$c_{\text{diff}} = \Delta c_{\text{diff}}. \quad (\text{S31})$$

This branch aligns the projected perturbation embedding with the batch-corrected expression level change using CLIP loss $\mathcal{L}_{\text{clip}} = \text{CLIP}(\Delta c_{\text{diff}}, z_p, \ell, z_{\text{src}})$.

3. **Regular Mode (regular):** The standard conditional mode combining both sequence-specific and null information:

$$c_{\text{diff}} = \Delta c_{\text{diff}} + c_{\text{diff}}^{\text{null}}. \quad (\text{S32})$$

Optimization Objectives. Given a timestep $t \in \{0, \dots, T\}$, the primary losses follow Section 3. The bridge matching loss trains the score network ϵ_θ to transport control latents to perturbed latents conditioned on the perturbation embedding:

$$\mathcal{L}_{\text{bridge}} = \mathbb{E}_{z_p, z_c, t} \left[\left\| \epsilon_\theta(z_t, t, u_p, z_c) - \epsilon^{\text{I2SB}} \right\|_2^2 \right], \quad (\text{S33})$$

where z_t is the bridge interpolant (Eq. 1) and u_p is conditioned through c_{diff} as described above. The reconstruction loss \mathcal{L}_{rec} evaluates the decoded prediction \hat{x}_p against the observed perturbed expression x_p using the hurdle log-normal likelihood (App. D). The alignment loss $\mathcal{L}_{\text{align}}$ is computed via the CLIP objective (App. C) during the source-conditional training mode.

Total Loss. The model is trained end-to-end by minimizing a weighted combination of losses (Section 3.4): $\mathcal{L} = \lambda_1 \mathcal{L}_{\text{bridge}} + \lambda_2 \mathcal{L}_{\text{align}} + \lambda_3 \mathcal{L}_{\text{rec}}$, where we utilize uncertainty weighting (Kendall et al., 2018) with learnable parameters σ_i to dynamically adjust each λ_i :

$$\mathcal{L}_{\text{total}} = \sum_i \frac{1}{2} \left(\frac{\mathcal{L}_i}{\sigma_i^2} + \log \sigma_i^2 \right). \quad (\text{S34})$$

F. Data and Evaluation Protocols

F.1. Dataset Statistics

We adopt the gene-level train/test splits from PerturbQA (Wu et al., 2025), which partitions perturbations such that test perturbation genes are entirely absent from training. This setup evaluates a model’s ability to generalize to novel genetic perturbations rather than interpolating among seen ones.

Low-Sample Setting. To simulate realistic data scarcity—where only limited observations exist for newly studied perturbations—we modify the zero-shot splits by transferring a small number of cells from the test set into training. Specifically, for each test perturbation gene, we randomly sample $k = 5$ cells and move them to the training set, providing minimal supervision while preserving the challenge of limited data.

This procedure yields the following train/test splits:

Dataset	Genes	Samples (Train / Test)
K562	4,136	318,443 / 61,233
Jurkat	6,842	155,393 / 36,073
RPE1	4,760	163,453 / 46,053
Combined	2,000	637,289 / 143,359

Table S3. Low-Sample dataset statistics. Train and test counts are reported as paired values.

Zero-Shot Setting. In the zero-shot setting, we use the original PerturbQA splits without modification. Models are trained exclusively on designated training perturbations and evaluated on held-out test perturbations without any access to test labels or test expression profiles during training.

Dataset	Perturb. (Train / Test)	Genes	Samples (Train / Test)
K562	1,564 / 267	4,136	317,103 / 62,573
Jurkat	1,227 / 313	6,842	153,823 / 37,643
RPE1	1,596 / 406	4,760	161,418 / 48,088
Combined	2,499 / 886	2,000	632,339 / 148,309

Table S4. Zero-shot dataset statistics. Train and test counts are reported as paired values.

Control Cell Partitioning. Control (unperturbed) cells serve as the reference distribution for computing perturbation effects. To prevent information leakage between training and evaluation, we partition control cells into two disjoint subsets:

- **Training controls (80%)**: Used during model training to compute perturbation effects for training genes and as input conditions for generative models.
- **Test controls (20%)**: Reserved for evaluation; used as input conditions when predicting responses to test perturbations.

This partitioning is performed randomly with a fixed seed for reproducibility. The same control partition is used across all methods to ensure fair comparison.

F.2. Metric Definitions

- *Mean Squared Error* (MSE), measuring pointwise reconstruction error across all genes. For N perturbations in the test set, let $\mathbf{p}_i \in \mathbb{R}^G$ denote the ground-truth pseudobulk expression and $\hat{\mathbf{p}}_i \in \mathbb{R}^G$ denote the predicted pseudobulk expression. We compute:

$$\text{MSE} = \frac{1}{N} \sum_{i=1}^N \|\hat{\mathbf{p}}_i - \mathbf{p}_i\|_2^2. \quad (\text{S35})$$

- *Direction Match* (Dir. Match), evaluating whether the predicted direction of change (up- or down-regulation) for differentially expressed (DE) genes is correct. For each perturbation t , G_t^\cap is the intersection of the predicted and true DE gene sets using an adjusted p -value threshold of 0.05. Given true log-fold changes $\Delta_{t,g}$ and predicted log-fold changes $\hat{\Delta}_{t,g}$, we compute:

$$\text{DirMatch}_t = \frac{\left| \left\{ g \in G_t^\cap : \text{sgn}(\hat{\Delta}_{t,g}) = \text{sgn}(\Delta_{t,g}) \right\} \right|}{|G_t^\cap|}. \quad (\text{S36})$$

- *Pearson correlation of expression change* (Δ_{Pearson}), measuring correlation between predicted and observed gene-wise perturbation effects. For each perturbation t , let the expression change Δ_t be the element-wise absolute difference between the mean expression of the perturbed cells $\bar{\mathbf{p}}_t$ and the control cells $\bar{\mathbf{c}}_t$: $\Delta_t = |\bar{\mathbf{p}}_t - \bar{\mathbf{c}}_t|$. Given the predicted expression change Δ^{pred} and true expression change Δ^{true} , we compute the Pearson correlation of expression change as:

$$\Delta_{\text{Pearson}} = \text{corr}(\Delta^{\text{pred}}, \Delta^{\text{true}}). \quad (\text{S37})$$

- *Precision@N* (Prec. @N), defined as the proportion of the top- N predicted DE genes that are truly significant. For each perturbation t , let $G_{t,\text{true}}^{(k)}$ and $G_{t,\text{pred}}^{(k)}$ denote the top- N true and predicted DE gene sets ranked by absolute log-fold change, respectively. We compute:

$$\text{Precision}_{t,N} = \frac{\left| G_{t,\text{true}}^{(N)} \cap G_{t,\text{pred}}^{(N)} \right|}{\left| G_{t,\text{pred}}^{(N)} \right|}. \quad (\text{S38})$$

- *Overlap@N* (Ov. @N), computing the overlap between predicted and ground-truth DE gene sets. For each perturbation t , we identify the top- N DE genes ranked by absolute log-fold change and compute the fraction of N genes present in both the predicted and ground truth gene sets:

$$\text{Overlap}_{t,N} = \frac{\left| G_{t,\text{pred}}^{(N)} \cap G_{t,\text{true}}^{(N)} \right|}{N}. \quad (\text{S39})$$

- *Discrimination Score (Cosine)* (Discr. Cos), a rank-based metric that assesses whether each predicted perturbation effect is most similar to its corresponding ground-truth effect (via cosine similarity) relative to all other perturbations (Wu et al., 2024). A higher score in this metric signifies a strong capacity to prevent mode collapse. Let $\mathcal{P} = \{1, \dots, T\}$ be the set of perturbations. For any $t, p \in \mathcal{P}$, let $\hat{\mathbf{y}}_t$ denote the predicted effect for perturbation t , and \mathbf{y}_p denote the ground-truth effect for perturbation mask \mathbf{m} . We define the cosine distance as:

$$d_{\text{cos}}(\hat{\mathbf{y}}_t, \mathbf{y}_p) = 1 - \frac{\hat{\mathbf{y}}_t^\top \mathbf{y}_p}{\|\hat{\mathbf{y}}_t\|_2 \|\mathbf{y}_p\|_2} \quad (\text{S40})$$

For each perturbation t , we count how many incorrect perturbations are closer to $\hat{\mathbf{y}}_t$ than the correct one:

$$r_t = \sum_{p \neq t} \mathbf{1}\{d_{\text{cos}}(\hat{\mathbf{y}}_t, \mathbf{y}_p) < d_{\text{cos}}(\hat{\mathbf{y}}_t, \mathbf{y}_t)\} \quad (\text{S41})$$

The final perturbation discrimination score is the normalized average rank across T perturbations:

$$\text{Discrimination Score} = 1 - \frac{1}{T} \sum_{t=1}^T \frac{r_t}{T-1} \quad (\text{S42})$$

- *Energy Distance*: To compare the distribution of real and predicted single-cell profiles for a given perturbation, we use the (unsquared) energy distance. For distributions P, Q over \mathbb{R}^d ,

$$\mathcal{E}(P, Q) = 2 \mathbb{E}\|\mathbf{X} - \mathbf{Y}\|_2 - \mathbb{E}\|\mathbf{X} - \mathbf{X}'\|_2 - \mathbb{E}\|\mathbf{Y} - \mathbf{Y}'\|_2, \quad (\text{S43})$$

For each dataset, we fit a PCA map $T(\cdot)$ (50 components) on the training split and compute a per-perturbation score $\hat{\mathcal{E}}(T(\mathbf{X}_g^{\text{real}}), T(\mathbf{X}_g^{\text{pred}}))$ using cells matching perturbation g . Energy distance is computed per-perturbation.

- *Pseudo-bulk mean R^2 .* Let G denote the number of genes. For a perturbation g , let $\mathbf{X}_g^{\text{real}} \in \mathbb{R}^{n_g \times G}$ and $\mathbf{X}_g^{\text{pred}} \in \mathbb{R}^{m_g \times G}$ denote the real and predicted gene expression matrices, with rows corresponding to cells and columns to genes. We form pseudo-bulk mean expression vectors by averaging across cells,

$$\boldsymbol{\mu}_g^{\text{real}} = \frac{1}{n_g} \sum_{i=1}^{n_g} \mathbf{X}_{g,i:}^{\text{real}}, \quad \boldsymbol{\mu}_g^{\text{pred}} = \frac{1}{m_g} \sum_{j=1}^{m_g} \mathbf{X}_{g,j:}^{\text{pred}}, \quad \boldsymbol{\mu}_g^{\text{real}}, \boldsymbol{\mu}_g^{\text{pred}} \in \mathbb{R}^G.$$

We compute the coefficient of determination across genes,

$$R_g^2 = 1 - \frac{\|\boldsymbol{\mu}_g^{\text{real}} - \boldsymbol{\mu}_g^{\text{pred}}\|_2^2}{\|\boldsymbol{\mu}_g^{\text{real}} - \bar{\boldsymbol{\mu}}_g^{\text{real}} \mathbf{1}\|_2^2}, \quad \bar{\boldsymbol{\mu}}_g^{\text{real}} = \frac{1}{G} \sum_{k=1}^G \boldsymbol{\mu}_{g,k}^{\text{real}},$$

where $\mathbf{1} \in \mathbb{R}^G$ is the all-ones vector. We compute R_g^2 for each perturbation and summarize results across perturbations for each method.

G. Detailed Performance Benchmarks

We provide the comprehensive breakdown of performance metrics across all datasets and settings.

Table S5. Low sample gene perturbation performance comparison Values are reported as mean \pm standard error. For readability, Ov. @N, Prec. @N, Dir. Match, and Disc. Cos are scaled by 10^{-1} , and MSE is scaled by 10^{-2} . Avg. Rank measures the overall rank averaged across all metrics. Best Avg. Rank is shown in **bold**.

Dataset	Method	Distributional Fidelity		DE Signal		Global Fit		Summary
		Discr. Cos \uparrow	E-Dist \downarrow	Dir. Match \uparrow	Prec. @N \uparrow	Ov. @N \uparrow	Δ Pearson \uparrow	
K562	BioLord	5.02 \pm 0.18	7.72 \pm 0.11	5.13 \pm 0.04	0.66 \pm 0.03	0.31 \pm 0.02	0.02 \pm 0.00	0.95 \pm 0.05
	GEARS	5.12 \pm 0.17	0.96 \pm 0.06	6.63 \pm 0.06	0.63 \pm 0.03	0.51 \pm 0.03	0.22 \pm 0.01	0.92 \pm 0.04
	Linear	5.04 \pm 0.18	7.56 \pm 0.10	3.58 \pm 0.05	0.18 \pm 0.01	0.51 \pm 0.02	0.11 \pm 0.00	0.81 \pm 0.04
	PerturbMean	5.02 \pm 0.18	7.56 \pm 0.10	8.50 \pm 0.05	0.15 \pm 0.01	0.64 \pm 0.03	0.55 \pm 0.01	0.78 \pm 0.04
	STATE	5.38 \pm 0.17	12.73 \pm 0.12	5.23 \pm 0.12	0.66 \pm 0.03	0.32 \pm 0.02	0.05 \pm 0.01	5.36 \pm 0.27
	STRAND	7.10 \pm 0.17	1.53 \pm 0.05	7.47 \pm 0.10	0.67 \pm 0.03	1.05 \pm 0.06	0.33 \pm 0.01	0.80 \pm 0.04
Jurkat	BioLord	5.07 \pm 0.16	8.48 \pm 0.13	6.13 \pm 0.06	0.44 \pm 0.03	0.18 \pm 0.02	0.14 \pm 0.00	0.95 \pm 0.05
	GEARS	5.64 \pm 0.17	1.27 \pm 0.07	6.71 \pm 0.06	0.40 \pm 0.03	0.23 \pm 0.02	0.24 \pm 0.01	0.86 \pm 0.05
	Linear	5.03 \pm 0.16	8.31 \pm 0.11	3.66 \pm 0.04	0.18 \pm 0.03	0.56 \pm 0.02	0.09 \pm 0.00	0.78 \pm 0.05
	PerturbMean	5.02 \pm 0.16	8.31 \pm 0.11	8.01 \pm 0.05	0.07 \pm 0.01	0.25 \pm 0.02	0.45 \pm 0.00	0.70 \pm 0.03
	STATE	6.52 \pm 0.17	13.57 \pm 0.20	5.84 \pm 0.11	0.45 \pm 0.03	0.20 \pm 0.02	0.13 \pm 0.01	4.54 \pm 0.15
	STRAND	7.19 \pm 0.16	1.82 \pm 0.07	7.58 \pm 0.09	0.44 \pm 0.03	0.64 \pm 0.04	0.34 \pm 0.01	0.78 \pm 0.04
RPE1	BioLord	5.03 \pm 0.14	11.24 \pm 0.21	6.72 \pm 0.05	0.99 \pm 0.04	0.63 \pm 0.03	0.26 \pm 0.01	1.99 \pm 0.08
	GEARS	5.41 \pm 0.15	2.36 \pm 0.11	7.59 \pm 0.08	1.00 \pm 0.04	1.36 \pm 0.06	0.44 \pm 0.01	1.62 \pm 0.06
	Linear	5.05 \pm 0.14	10.25 \pm 0.15	4.31 \pm 0.05	2.17 \pm 0.07	1.73 \pm 0.05	0.33 \pm 0.01	1.55 \pm 0.06
	PerturbMean	5.01 \pm 0.14	10.26 \pm 0.15	8.69 \pm 0.05	0.37 \pm 0.02	0.80 \pm 0.02	0.57 \pm 0.01	1.46 \pm 0.06
	STATE	6.97 \pm 0.14	11.42 \pm 0.19	6.03 \pm 0.08	1.02 \pm 0.04	0.57 \pm 0.03	0.19 \pm 0.01	5.27 \pm 0.07
	STRAND	7.04 \pm 0.14	2.62 \pm 0.10	7.93 \pm 0.08	1.01 \pm 0.04	1.76 \pm 0.07	0.47 \pm 0.01	1.39 \pm 0.05

Table S6. Zero-shot gene perturbation performance comparison Values are reported as mean \pm standard error. For readability, Ov. @N, Prec. @N, Dir. Match, and Disc. Cos are scaled by 10^{-1} , and MSE is scaled by 10^{-2} . (N/A) represents that the method does not apply to the task and is therefore not evaluated. Avg. Rank measures the overall rank averaged across all metrics. Best Avg. Rank is shown in **bold**.

Dataset	Method	Distributional Fidelity		DE Signal		Global Fit		Summary
		Discr. Cos \uparrow	E-Dist \downarrow	Dir. Match \uparrow	Prec. @N \uparrow	Ov. @N \uparrow	Δ Pearson \uparrow	
K562	BioLord	5.07 \pm 0.18	7.70 \pm 0.11	5.31 \pm 0.04	0.68 \pm 0.03	0.31 \pm 0.02	0.04 \pm 0.00	0.92 \pm 0.05
	Linear	5.06 \pm 0.18	7.56 \pm 0.10	3.46 \pm 0.05	0.18 \pm 0.01	0.49 \pm 0.02	0.11 \pm 0.00	0.78 \pm 0.04
	PerturbMean	5.02 \pm 0.18	7.56 \pm 0.10	8.50 \pm 0.05	0.15 \pm 0.01	0.64 \pm 0.03	0.55 \pm 0.01	0.78 \pm 0.04
	STATE	N/A	N/A	N/A	N/A	N/A	N/A	N/A
	STRAND	5.14 \pm 0.18	1.74 \pm 0.08	6.58 \pm 0.10	0.69 \pm 0.03	0.85 \pm 0.04	0.21 \pm 0.01	0.85 \pm 0.04
								1.57
Jurkat	BioLord	5.05 \pm 0.16	8.51 \pm 0.13	5.88 \pm 0.04	0.46 \pm 0.03	0.20 \pm 0.02	0.10 \pm 0.00	0.84 \pm 0.04
	Linear	5.02 \pm 0.16	8.31 \pm 0.11	3.56 \pm 0.04	0.17 \pm 0.03	0.56 \pm 0.02	0.09 \pm 0.00	0.72 \pm 0.03
	PerturbMean	5.02 \pm 0.16	8.31 \pm 0.11	8.01 \pm 0.05	0.07 \pm 0.01	0.25 \pm 0.02	0.45 \pm 0.00	0.70 \pm 0.03
	STATE	N/A	N/A	N/A	N/A	N/A	N/A	N/A
	STRAND	5.26 \pm 0.16	1.97 \pm 0.09	7.04 \pm 0.09	0.46 \pm 0.03	0.52 \pm 0.04	0.29 \pm 0.01	0.76 \pm 0.03
								1.86
RPE1	BioLord	5.04 \pm 0.14	11.29 \pm 0.21	6.90 \pm 0.06	1.08 \pm 0.04	0.74 \pm 0.03	0.26 \pm 0.01	1.92 \pm 0.08
	Linear	5.02 \pm 0.14	10.26 \pm 0.15	4.27 \pm 0.05	2.19 \pm 0.07	1.73 \pm 0.05	0.33 \pm 0.01	1.47 \pm 0.06
	PerturbMean	5.01 \pm 0.14	10.28 \pm 0.15	8.69 \pm 0.05	0.37 \pm 0.02	0.80 \pm 0.02	0.57 \pm 0.01	1.46 \pm 0.06
	STATE	N/A	N/A	N/A	N/A	N/A	N/A	N/A
	STRAND	5.13 \pm 0.14	3.13 \pm 0.14	7.86 \pm 0.08	1.09 \pm 0.04	1.84 \pm 0.07	0.48 \pm 0.01	1.53 \pm 0.06
								1.71

Dataset	Method	Discr. Cos \uparrow	E-Dist \downarrow	Dir. Match \uparrow	Prec. @N \uparrow	Ov. @N \uparrow	Δ Pearson \uparrow	MSE \downarrow	Avg. Rank \downarrow
K562	BioLord	5.06 \pm 0.22	7.72 \pm 0.13	5.28 \pm 0.04	0.70 \pm 0.04	0.32 \pm 0.03	0.04 \pm 0.00	0.93 \pm 0.06	4.14
	GEARS	4.82 \pm 0.21	1.01 \pm 0.08	6.57 \pm 0.06	0.69 \pm 0.04	0.56 \pm 0.03	0.21 \pm 0.01	0.90 \pm 0.05	2.86
	Linear	5.08 \pm 0.21	7.58 \pm 0.12	3.48 \pm 0.05	0.20 \pm 0.02	0.50 \pm 0.02	0.11 \pm 0.00	0.80 \pm 0.05	3.57
	PerturbMean	4.80 \pm 0.21	7.58 \pm 0.12	8.43 \pm 0.05	0.15 \pm 0.01	0.66 \pm 0.03	0.54 \pm 0.01	0.79 \pm 0.05	2.57
	STATE	N/A	N/A	N/A	N/A	N/A	N/A	N/A	N/A
	STRAND	5.15 \pm 0.22	1.70 \pm 0.09	6.53 \pm 0.12	0.71 \pm 0.04	0.87 \pm 0.05	0.21 \pm 0.02	0.86 \pm 0.05	1.86
Jurkat	BioLord	5.18 \pm 0.19	8.63 \pm 0.16	5.90 \pm 0.04	0.48 \pm 0.04	0.21 \pm 0.03	0.10 \pm 0.00	0.87 \pm 0.05	3.86
	GEARS	5.77 \pm 0.20	1.40 \pm 0.09	6.84 \pm 0.07	0.46 \pm 0.04	0.26 \pm 0.03	0.26 \pm 0.01	0.83 \pm 0.04	2.57
	Linear	5.13 \pm 0.19	8.42 \pm 0.13	3.57 \pm 0.05	0.18 \pm 0.03	0.56 \pm 0.02	0.10 \pm 0.01	0.75 \pm 0.04	3.57
	PerturbMean	4.97 \pm 0.19	8.41 \pm 0.13	7.99 \pm 0.06	0.08 \pm 0.01	0.24 \pm 0.02	0.45 \pm 0.01	0.74 \pm 0.04	2.86
	STATE	N/A	N/A	N/A	N/A	N/A	N/A	N/A	N/A
	STRAND	5.35 \pm 0.19	1.92 \pm 0.10	7.12 \pm 0.09	0.48 \pm 0.04	0.53 \pm 0.05	0.29 \pm 0.01	0.79 \pm 0.04	2.14
RPE1	BioLord	5.13 \pm 0.17	11.58 \pm 0.25	6.93 \pm 0.06	1.15 \pm 0.05	0.79 \pm 0.04	0.27 \pm 0.01	2.00 \pm 0.09	3.86
	GEARS	5.08 \pm 0.18	4.12 \pm 0.22	5.10 \pm 0.04	1.00 \pm 0.05	0.72 \pm 0.04	0.01 \pm 0.01	2.29 \pm 0.10	4.29
	Linear	5.25 \pm 0.17	10.40 \pm 0.18	4.34 \pm 0.06	2.31 \pm 0.08	1.80 \pm 0.06	0.35 \pm 0.01	1.51 \pm 0.07	2.57
	PerturbMean	5.21 \pm 0.17	10.42 \pm 0.18	8.67 \pm 0.07	0.39 \pm 0.02	0.84 \pm 0.03	0.58 \pm 0.01	1.51 \pm 0.07	2.57
	STATE	N/A	N/A	N/A	N/A	N/A	N/A	N/A	N/A
	STRAND	5.30 \pm 0.18	3.06 \pm 0.16	7.95 \pm 0.10	1.17 \pm 0.05	1.99 \pm 0.09	0.50 \pm 0.02	1.55 \pm 0.07	1.71

Table S7. Zero-shot performance comparison with GEARS. We selected the subset of genes that available for GEARS to make prediction. 189 genes for K562, 236 genes for Jurkat, and 269 genes for RPE1.

Dataset	Method	Discr. Cos \uparrow	E-Dist \downarrow	Dir. Match \uparrow	Prec. @N	Ov. @N \uparrow	Δ Pearson \uparrow	MSE \downarrow	Avg. Rank \downarrow
K562	STRAND (w/o CLIP)	6.81 \pm 0.17	1.42 \pm 0.05	7.34 \pm 0.11	0.67 \pm 0.03	1.01 \pm 0.05	0.34 \pm 0.01	0.76 \pm 0.04	1.57
	STRAND	7.10 \pm 0.17	1.53 \pm 0.05	7.47 \pm 0.10	0.67 \pm 0.03	1.05 \pm 0.06	0.33 \pm 0.01	0.80 \pm 0.04	1.43
Jurkat	STRAND (w/o CLIP)	6.73 \pm 0.16	1.64 \pm 0.07	7.50 \pm 0.09	0.44 \pm 0.03	0.61 \pm 0.05	0.34 \pm 0.01	0.76 \pm 0.04	1.57
	STRAND	7.19 \pm 0.16	1.82 \pm 0.07	7.58 \pm 0.09	0.44 \pm 0.03	0.64 \pm 0.04	0.34 \pm 0.01	0.78 \pm 0.04	1.43
RPE1	STRAND (w/o CLIP)	6.23 \pm 0.15	2.84 \pm 0.12	7.78 \pm 0.09	0.99 \pm 0.04	1.75 \pm 0.07	0.46 \pm 0.02	1.53 \pm 0.06	2.00
	STRAND	7.04 \pm 0.14	2.62 \pm 0.10	7.93 \pm 0.08	1.01 \pm 0.04	1.76 \pm 0.07	0.47 \pm 0.01	1.39 \pm 0.05	1.00

Table S8. Ablation on CLIP loss

H. State-of-the-art Baselines

We compare our method against the following three SOTA models: **GEARS** (Roohani et al., 2023), **BioLord** (Piran et al., 2024), **STATE** (Adduri et al., 2025b), and two baseline models: **Linear** model on Borzoi embeddings (Linder et al., 2025), and **PerturbMean** (Viñas Torné et al., 2025).

GEARS (Roohani et al., 2023) GEARS is a graph neural network that integrates gene–gene coexpression and GO-derived perturbation similarity graphs to learn perturbation embeddings and predict post-perturbation gene expression. It represents the dominant paradigm of incorporating *gene-level biological priors*, allowing us to test whether sequence-resolved DNA conditioning provides advantages beyond relational gene graphs.

We used the default GO-based perturbation similarity graph from the official GEARS implementation, with $k = 20$ neighbors for perturbation embedding learning. GEARS was trained for 20 epochs using a hidden size of 64 and a learning rate of 10^{-3} . Because perturbation embeddings are defined over the GO graph, GEARS is limited to perturbations whose target genes are present in the training graph.

BioLord (Piran et al., 2024) BioLord is a disentanglement-based variational autoencoder that factorizes gene expression into cellular context and perturbation components, enabling counterfactual prediction of perturbation effects.

To introduce functional context, we incorporate GO-derived perturbation neighborhood features from the GEARS GO graph. For each perturbation, we select the top 20 GO neighbors ranked by edge importance and use these weighted neighborhood features as ordered attributes for conditioning. BioLord was trained for 200 epochs using AdamW for each dataset.

STATE (Adduri et al., 2025b) STATE is a transformer-based foundation model trained on over 100M perturbed cells, representing the frontier of scale in expression-based perturbation modeling.

We extracted basal cell embeddings using the pretrained 600M-parameter STATE embedding model (epoch-16 checkpoint from the original work). A STATE transition model was then trained from scratch using default hyperparameters to predict perturbed expression from basal embeddings, preventing data leakage from overlapping Reppogle datasets. Evaluation of STATE was restricted to low-sample settings, as the original work does not benchmark zero-shot prediction of unseen perturbations within a cell line.

Linear We include a linear regression model trained on Borzoi (Linder et al., 2025) DNA embeddings (7 kb TSS-centered context, mean-pooled) to isolate the contribution of sequence information under minimal architectural assumptions. Recent benchmarks indicate that such linear models can be competitive in perturbation prediction (Ahmann-Eltze et al., 2025). Implementation details are provided in App. I.1.

PerturbMean (Viñas Torné et al., 2025) PerturbMean predicts the average perturbation effect observed during training and serves as a strong non-parametric baseline. Systema demonstrated that this baseline often matches or exceeds GEARS, scGPT, and CPA, making it a useful reference for assessing whether models capture perturbation-specific effects beyond systematic variation.

Following the evaluation framework of Viñas Torné et al. (2025), we employ the perturbed mean as a nonparametric baseline. Let $\mathcal{P}_{\text{train}}$ denote the set of all perturbed cells in the training data, and let $\mathbf{x}_i \in \mathbb{R}^n$ denote the gene expression profile of cell i . The perturbed mean is defined as

$$\boldsymbol{\mu}_{\text{pert}} = \frac{1}{|\mathcal{P}_{\text{train}}|} \sum_{i \in \mathcal{P}_{\text{train}}} \mathbf{x}_i. \quad (\text{S44})$$

This baseline uses $\boldsymbol{\mu}_{\text{pert}}$ as the predicted post-perturbation expression profile for all test perturbations, regardless of the specific gene targeted. The predicted perturbation effect is then computed as

$$\widehat{\Delta \mathbf{x}} = \boldsymbol{\mu}_{\text{pert}} - \boldsymbol{\mu}_{\text{ctrl}}, \quad (\text{S45})$$

where $\boldsymbol{\mu}_{\text{ctrl}}$ is the mean expression of control cells. This prediction is compared against the ground-truth perturbation effect $\Delta \mathbf{x}$ for each held-out perturbation X .

H.1. RNA representation pipeline (applies to STRAND and STATE)

Both STRAND and STATE leverage a pretrained RNA foundation model to obtain cell embeddings. To preserve maximal transcriptome information at the representation stage, we compute RNA embeddings from the *full* gene expression matrix (no HVG selection or gene filtering beyond dataset-provided gene definitions). For downstream perturbation prediction and evaluation (e.g., pseudobulk shifts and metrics), we operate on the Standardized expression matrix described below.

Standardized expression matrices. For each cell line (K562, RPE1, Jurkat), we build an `AnnData` object with a consistent gene axis defined by a canonical gene list (either cell-line-specific or the across-cell-line union; see `reformat_adata_genes`). All preprocessing starts from the raw count matrix X .

Per-cell library-size normalization. For each dataset we normalize (the per-cell-line files and the final combined HVG matrix), we apply Scanpy's library-size normalization with `sc.pp.normalize_total(adata, target_sum=1e4)`, which rescales each cell's total UMI count to 10,000. For cell i with total count c_i , each gene count x_{ij} is transformed as

$$x'_{ij} = x_{ij} \cdot \frac{10,000}{c_i}.$$

Logarithmic transformation. After library-size normalization, we apply a log transform using `sc.pp.log1p(adata)`:

$$x''_{ij} = \log(1 + x'_{ij}).$$

This stabilizes variance and limits the influence of extreme counts.

HVG selection for the cross-cell-line (Combined) dataset. To construct the final combined dataset, we concatenate union-gene raw count matrices across cell lines and select highly variable genes using only control cells. We run `sc.pp.highly_variable_genes(..., flavor="seurat_v3", n_top_genes=2000)` on the raw counts to avoid selecting genes whose variance is driven by perturbations. We then restrict the full concatenated matrix to these 2,000 HVGs. Only after HVG selection do we apply library-size normalization to 10,000 counts per cell followed by `log1p`, yielding the expression matrix used for downstream analyses.

For the combined cross-cell-line dataset, HVG selection is performed prior to normalization and log transformation, whereas per-cell-line datasets are normalized directly without HVG restriction.

I. Other baselines

I.1. Linear Baseline

The linear baseline model is based on the assumption that the effect of a perturbation can be approximated as a linear transformation of the perturbed gene's characteristics and the cell's covariates, learned as an additive shift to the cell's baseline state.

Model Formulation. Let $x_i \in \mathbb{R}^G$ denote the gene expression profile of cell i under a perturbation g (where G is the number of genes), and let $x_{i,\text{base}} \in \mathbb{R}^G$ denote the corresponding baseline expression profile. In our experimental setup, $x_{i,\text{base}}$ corresponds to the expression of a control cell (no perturbation) matched to the sample i , or the mean expression of control cells if direct matching is unavailable.

We formalize the prediction task as learning the perturbation effect $\delta_i \in \mathbb{R}^G$, defined as the residual between the perturbed and baseline states:

$$\delta_i = x_i - x_{i,\text{base}} \quad (\text{S46})$$

The model constructs a feature vector z_i for each sample. For single-dataset experiments, z_i consists solely of the semantic embedding of the perturbed gene $e_g \in \mathbb{R}^D$. For the case of the combined dataset that consists of multiple cell lines, we augment the feature vector with the cell line identity as a one-hot encoded covariate c_i to account for cell-type specific baseline shifts:

$$z_i = \begin{cases} e_g & \text{single dataset} \\ [e_g; c_i] & \text{combined dataset} \end{cases} \quad (\text{S47})$$

In cases where the sample is a control (no perturbation), we utilize a zero vector for the gene embedding component e_g .

The predicted perturbation shift $\hat{\delta}_i \in \mathbb{R}^G$ is computed via a learned linear projection:

$$\hat{\delta}_i = W z_i + b \quad (\text{S48})$$

where W is the weight matrix mapping the feature space to the gene expression space, and $b \in \mathbb{R}^G$ is the bias vector.

The final predicted expression profile \hat{x}_i is obtained by applying the predicted shift to the baseline:

$$\hat{x}_i = x_{i,\text{base}} + \hat{\delta}_i \quad (\text{S49})$$

Training and Implementation. The parameters W and b are estimated using Lasso regression (Linear least squares with L_1 regularization) to minimize the mean squared error between the predicted shifts $\hat{\delta}$ and the observed shifts δ , while enforcing sparsity in the weight matrix. The objective function minimizes:

$$\mathcal{L} = \sum_i \|\delta_i - (W z_i + b)\|_2^2 + \alpha \|W\|_1 \quad (\text{S50})$$

where α is the regularization strength (defaulting to $\alpha = 0.05$). Prior to training, both the input features z and the target residuals δ are standardized using Z-score normalization.

I.2. Concatenation-Based Conditioning Baseline

To assess whether the performance gains of STRAND arise from conditioning the diffusion dynamics rather than increased model capacity, we implement a concatenation-based baseline that replaces transport-based conditioning with feature fusion. This baseline mirrors common conditioning strategies used in prior perturbation prediction methods.

I.3. Input Representations

Let $z_c \in \mathbb{R}^d$ denote the latent embedding of a control cell, obtained from the same pretrained RNA encoder used in STRAND. Let $E_s \in \mathbb{R}^{L \times d_0}$ denote the token-level DNA embeddings produced by Borzoi for the genomic region associated with the perturbation. As in STRAND, a learnable perturbation adaptor f_ϕ maps E_s to a fixed-dimensional perturbation embedding:

$$z_{\text{DNA}} = f_\phi(E_s) \in \mathbb{R}^d.$$

At inference time, the baseline observes only (z_c, z_{DNA}) .

I.4. Concatenation Predictor Architecture

The concatenation baseline predicts the perturbed cell embedding \hat{z}_p via a deterministic feedforward network:

$$\hat{z}_p = g_\psi([z_c ; z_{\text{DNA}}]),$$

where $[\cdot ; \cdot]$ denotes vector concatenation and $g_\psi : \mathbb{R}^{2d} \rightarrow \mathbb{R}^d$ is a multilayer perceptron.

The predictor g_ψ consists of:

- An input layer of dimension $2d$
- Two hidden layers with ReLU activations
- An output layer of dimension d

The hidden layer widths are matched to the diffusion score network used in STRAND to control for parameter count.

I.5. Gene-Level Expression Reconstruction

The predicted perturbed embedding \hat{z}_p is passed to the same gene-level decoder used in STRAND, which reconstructs gene expression values via the hurdle truncated Gaussian residual likelihood. This ensures that differences in performance arise solely from the conditioning mechanism, not from downstream decoding.

I.6. Training Objective

The concatenation baseline is trained without any diffusion or bridge-matching objective. The reconstruction loss \mathcal{L}_{rec} is the same hurdle truncated Gaussian likelihood used in STRAND. The same contrastive loss between z_{DNA} and perturbed embeddings is included to ensure comparable supervision.

We apply the same uncertainty weighting as STRAND to balance the active objectives:

$$\mathcal{L}_{\text{total}} = \sum_{i \in \{\text{rec, CLIP}\}} \frac{1}{2} \left(\frac{\mathcal{L}_i}{\sigma_i^2} + \log \sigma_i^2 \right),$$

where σ_i are learnable uncertainty parameters. Note that, unlike STRAND, the diffusion losses are absent; only the reconstruction and contrastive terms participate in the weighting.

J. Additional Results and Case Studies

J.1. Unseen Cell-Line Perturbation Prediction

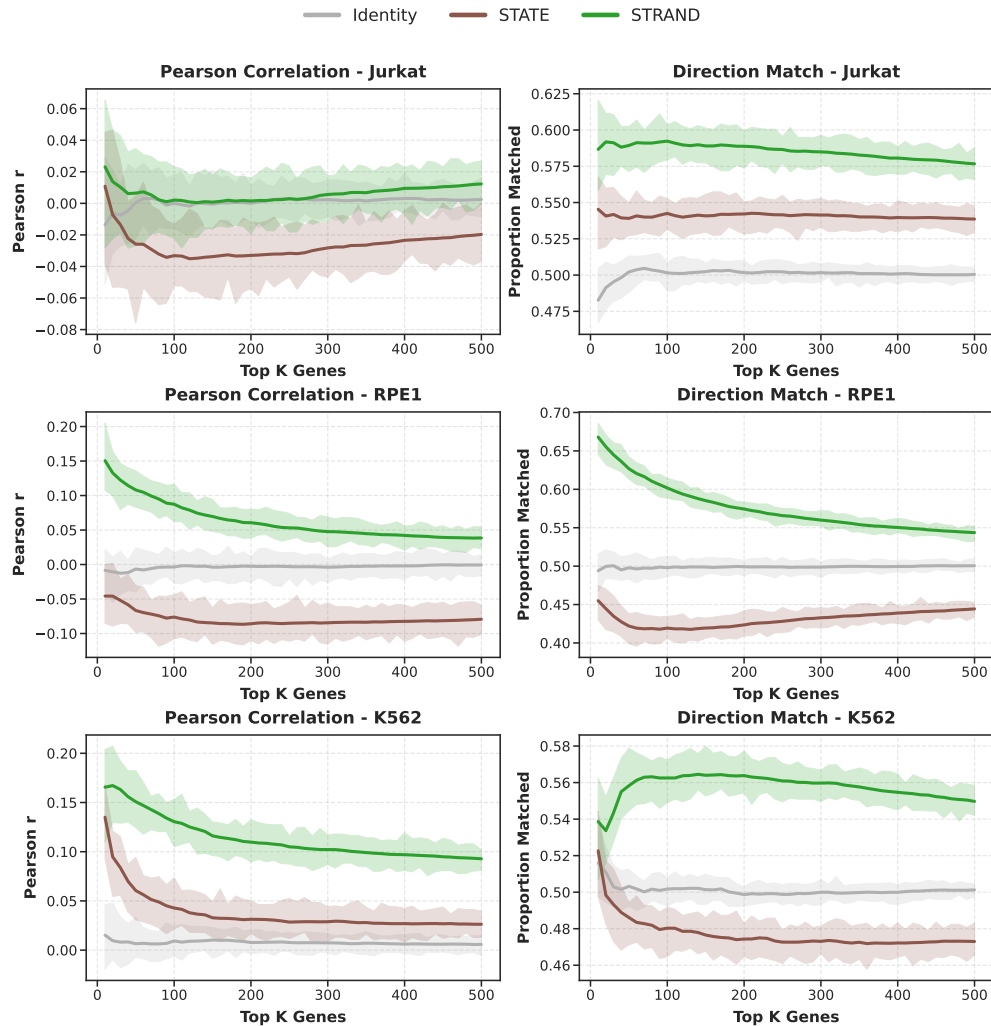


Figure S1. Unseen cell-line perturbation prediction. STRAND (green) consistently outperforms STATE (pink) and the Identity baseline (gray).

J.2. Case Studies

Table S9. Sequence-level perturbation impact across FLVCR1 TSSs in K562. Among five candidate TSSs, the alternative FLVCR1b promoter (Transcript 202) exhibits the largest perturbation impact, measured by Energy Distance.

Transcript ID	Transcript Annotation		Impact E-dist. ↑
	TSS (chr1)	Type	
201	212,858,275	Canonical (FLVCR1a)	0.564
202	212,858,916	Alternative (FLVCR1b)	0.683
203	212,864,412	Unknown	0.450
204	212,883,409	Unknown	0.580
205	212,863,631	Unknown	0.470

CD3D in Jurkat cells. CD3D encodes a component of the T-cell receptor complex and is specifically expressed in T lymphocytes. Jurkat, a T-cell leukemia line, shows dramatically higher perturbation sensitivity across the CD3D locus compared to K562 and RPE1 (Figure 6). The elevated baseline and multiple peaks throughout the gene body suggest that Jurkat cells maintain active regulatory architecture at this locus, consistent with CD3D's essential role in T-cell signaling (Alarcon et al., 1991). The peaks observed at approximately 1kb and 5–6kb downstream of the TSS may correspond to intronic enhancers or other cis-regulatory elements active specifically in the T-cell context.

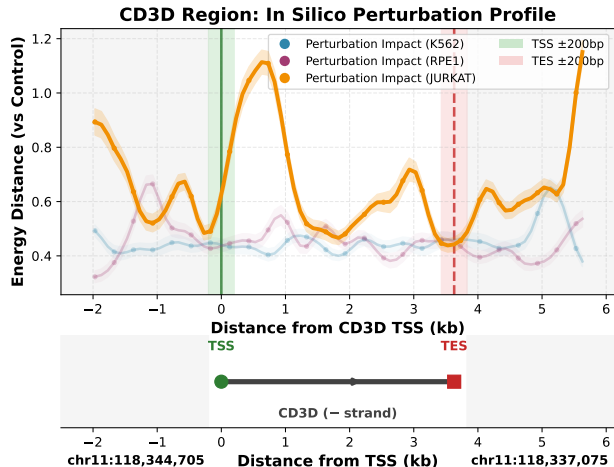


Figure S2. Jurkat - CD3D.

KRT18 in RPE1 cells. KRT18 (Keratin 18) is an intermediate filament protein characteristic of simple epithelia. RPE1, a retinal pigment epithelial cell line, shows the strongest perturbation response at this locus, with prominent peaks near the TSS and in the downstream region around 5kb (Figure S3). In contrast, the hematopoietic lines K562 and Jurkat show substantially lower and flatter profiles. This pattern recapitulates KRT18's known epithelial-specific expression pattern (Hunt & Davis, 1990). Interestingly, the downstream peak in RPE1 cells (approximately 5kb from TSS) shows even higher sensitivity than the TSS itself, suggesting the presence of a strong distal regulatory element that may be critical for KRT18 expression in epithelial cells.

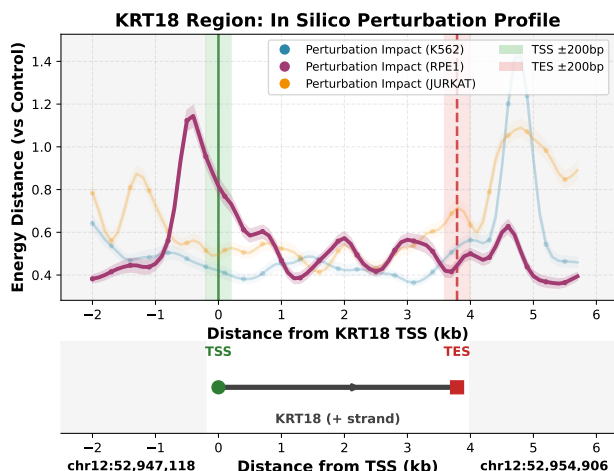


Figure S3. RPE1 - KRT18.

These results show that STRAND captures biologically meaningful cell-type-specific regulatory landscapes without explicit supervision on chromatin accessibility or transcription factor binding data. The approach recovers known regulatory patterns at canonical sites (e.g., TSS regions) and highlights putative novel regulatory elements (particularly the intragenic and downstream peaks) that could guide experimental prioritization for functional validation studies.

K. Limitations and Future Work

Limitations. Our *in silico* sequence perturbation experiments do not account for practical constraints such as sgRNA design feasibility or target druggability, which may limit experimental realizability. We also assume perturbations occur at canonical transcription start sites and model them using a fixed ± 200 bp window; this coarse approximation ignores fine-grained sgRNA positioning and sequence-specific targeting effects. In addition, the regulatory context window supported by STRAND is unavoidably capped by the capacity of the upstream DNA foundation model. Finally, the current model is trained exclusively on CRISPRi perturbation data; while the framework is readily extensible, we have not evaluated performance on other perturbation modalities (such as CRISPRa).

Future Work. Several promising directions remain. Integrating alternative DNA and RNA foundation models may improve representation quality and generalization. Incorporating long-range regulatory interactions, such as distal enhancers and chromatin contacts, would enable more comprehensive modeling of sequence-to-expression relationships. Cross-context generalization also remains limited by data scale; we anticipate improved performance as larger, more diverse perturbation datasets across additional cell types become available.